Cancer-Associated Fibroblasts Expressing Sulfatase 1 Facilitate VEGFA-Dependent Microenvironmental Remodeling to Support Colorectal Cancer

Huijuan Wang[1,2,3], Jiaxin Chen[1,2,3], Xiaoyu Chen[1,2,3], Yingqiang Liu[1,2,3], Jiawei Wang[1,2,3], Qing Meng[1,2,3], Huogang Wang[1,2,3], Ying He[4], Yujia Song[5], Jingyun Li[1,2,3], Zhenyu Ju[6], Peng Xiao[7], Junbin Qian[8,9], and Zhangfa Song[1,2,3]

ABSTRACT

Tumor stroma plays a critical role in fostering tumor progression and metastasis. Cancer-associated fibroblasts (CAF) are a major component of the tumor stroma. Identifying the key molecular determinants for the protumor properties of CAFs could enable the development of more effective treatment strategies. In this study, through analyses of single-cell sequencing data, we identified a population of CAFs expressing high levels of sulfatase 1 (*SULF1*), which was associated with poor prognosis in patients with colorectal cancer. Colorectal cancer models using mice with conditional SULF1 knockout in fibroblasts revealed the tumor-supportive function of SULF1$^+$ CAFs. Mechanistically, SULF1$^+$ CAFs enhanced the release of VEGFA from heparan sulfate proteoglycan. The increased bioavailability of VEGFA initiated the deposition of extracellular matrix and enhanced angiogenesis. In addition, intestinal microbiota–produced butyrate suppressed SULF1 expression in CAFs through its histone deacetylase (HDAC) inhibitory activity. The insufficient butyrate production in patients with colorectal cancer increased the abundance of SULF1$^+$ CAFs, thereby promoting tumor progression. Importantly, tumor growth inhibition by HDAC was dependent on SULF1 expression in CAFs, and patients with colorectal cancer with more SULF1$^+$ CAFs were more responsive to treatment with the HDAC inhibitor chidamide. Collectively, these findings unveil the critical role of SULF1$^+$ CAFs in colorectal cancer and provide a strategy to stratify patients with colorectal cancer for HDAC inhibitor treatment.

Significance: SULF1$^+$ cancer-associated fibroblasts play a tumor-promoting role in colorectal cancer by stimulating extracellular matrix deposition and angiogenesis and can serve as a biomarker for the therapeutic response to HDAC inhibitors in patients.

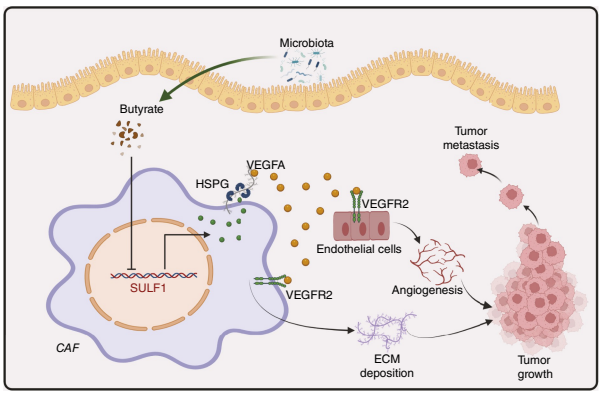

Introduction

Colorectal cancer has the third highest incidence and mortality rates among malignant tumors in the world (1, 2). The majority patients with colorectal cancer have distant metastasis at the time of diagnosis and miss the opportunity for radical surgery; in addition, their 5-year survival rate remains considerably low (3, 4). Identification of new molecular mechanisms that affect the progression and prognosis of colorectal cancer and exploring new targets for colorectal cancer treatment have always been the focus of research in the field of oncology (4, 5).

Cancer-associated fibroblasts (CAF), the most important cellular component in the tumor microenvironment (TME), play a critical role

[1]Department of Colorectal Surgery, Sir Run Run Shaw Hospital, Zhejiang University School of Medicine, Hangzhou, China. [2]Key Laboratory of Biological Treatment of Zhejiang Province, Hangzhou, China. [3]Key Laboratory of Integrated Traditional Chinese and Western Medicine Research on Anorectal Diseases of Zhejiang Province, Hangzhou, China. [4]Huzhou Key Laboratory of Translational Medicine, Huzhou, China. [5]Hangzhou No. 14 High School, Hangzhou, China. [6]Key Laboratory of Regenerative Medicine of Ministry of Education, Guangzhou Regenerative Medicine and Health Guangdong Laboratory, Institute of Ageing and Regenerative Medicine, Jinan University, Guangzhou, China. [7]Department of Gastroenterology, Sir Run Run Shaw Hospital, Zhejiang University School of Medicine, Hangzhou, China. [8]Zhejiang Key Laboratory of Precision Diagnosis and Therapy for Major Gynecological Diseases, Women's Hospital, Zhejiang University School of Medicine, Hangzhou, China. [9]Zhejiang Provincial Clinical Research Center for Child Health, Hangzhou, China.

Corresponding Authors: Zhangfa Song, Department of Colorectal Surgery, Sir Run Run Shaw Hospital, No. 3 East Qingchun Road, Hangzhou 310016, China. Email: songzhangfa@zju.edu.cn; Junbin Qian, Zhejiang Key Laboratory of Precision Diagnosis and Therapy for Major Gynecological Diseases, Women's Hospital, Zhejiang University School of Medicine, Hangzhou 310058, China. Email: dr_qian@zju.edu.cn; and Peng Xiao, Department of Gastroenterology, Sir Run Run Shaw Hospital, Zhejiang University School of Medicine, Hangzhou 310016, China. Email: tulipxp@zju.edu.cn

Cancer Res 2024;XX:XX–XX

doi: 10.1158/0008-5472.CAN-23-3987

in the pathogenesis of tumors (6). CAFs affect tumor progression by regulating the homeostasis of tumor extracellular matrix (ECM), changing secretion profiles, and regulating metabolism (7–9). Therefore, it is crucial to examine how CAFs affect tumor progression and the specific underlying mechanisms involved.

Studies have shown that there is substantial heterogeneity in CAFs. Some CAFs may have greater oncogenic potential, such as the ability to induce stronger metastasis or invasion or be more likely to develop drug resistance (10–12). In contrast, some CAF subsets have also been reported to inhibit tumor progression (13). The main reasons for the heterogeneity of CAFs include the different origins of CAFs and the dynamic transformation of individual CAF populations between tumor-promoting or tumor-suppressing phenotypes owing to the complex composition of the TME, in addition to the existence of a broad subpopulation of CAFs with different functions (14). Recently, single-cell sequencing technologies have greatly facilitated the dissection of tumor heterogeneity. By obtaining dynamic genomic and transcriptomic data from single cells at a specific stage or site, this technology enables the comprehensive genetic analysis of tumor tissues and cell subtypes. In addition, it can be employed to discover abnormally proliferating cell types in search of new pathogenic mechanisms (15–17).

Sulfatase 1 (SULF1) is a recently discovered member of the sulfatase family. It is located on cell surface and regulates cell functions by altering the sulfated state of heparan sulfate proteoglycans (HSPG), a crucial ECM component (18, 19). HSPGs can bind to a variety of protein ligands, including growth factors, growth factor receptors, cytokines, chemokines, and cell-adhesion factors, thereby regulating a variety of physiologic and pathologic processes (18, 20, 21). It has been reported that SULF1 plays the role of a tumor suppressor in liver cancer, ovarian cancer, and head and neck tumors. Tumor cells transfected with SULF1 have a considerable ability to proliferate and metastasize (22–24). In contrast, the cancer-promoting effects of SULF1 have also been reported. For example, high expression of SULF1 can promote the proliferation of liver cancer cells *in vitro*, and SULF1 is related to a poor prognosis in patients with bladder and urothelial cancer (25, 26). However, previous studies have investigated only the function of SULF1 in tumor cells, its potential role in regulating tumor stroma remains unclear.

The gut microbiota produces many short-chain fatty acids (SCFA) through the fermentation of dietary fiber, and the main SCFAs present at concentrations above 100 mmol/L include propionate, acetate, and butyrate (27, 28). SCFAs have been shown to influence the progression of various diseases such as inflammatory bowel disease, diabetes, atherosclerosis, and colorectal cancer (29–32). SCFAs can mainly affect the function of tumor cells or immune cells by binding to G protein–coupled receptors or acting as histone deacetylase inhibitors (HDACi; refs. 33–35).

Here, for the first time, we identified SULF1 as a key gene driving the protumor properties of colorectal cancer–associated CAFs. The detailed mechanisms were further investigated in depth. In addition, a previously unidentified role of butyrate, a major SCFA in the gut, was revealed in regulating the SULF1 expression in CAFs.

Materials and Methods

Single-cell transcriptomic analysis

Gene expression matrices from the GSE144735 and GSE132465 datasets were independently clustered using the Seurat package (v4.1.1). The data analyzed in this study were obtained from Gene Expression Omnibus at GSE144735 and GSE132465. At the "scale data" step, we regressed out confounding factors: the number of features, number of counts, percentage of mitochondrial RNA, patient ID and cell cycle (S and G_2–M phase scores calculated by the CellCycleScoring function in Seurat), IFN score, dissociation stress score, and hypoxia score (calculated by the AddModuleScore function with respective gene signatures). This step was followed by routine principal component analysis, graph-based clustering, and marker gene–based major cell-type annotation. Cell doublets were estimated using both scrublet (v0.2.3) and Doublet Finder (v2.0.3), with an expected doublet rate of 0.05 and clustered for 20 principal components. For fibroblast subtype analysis, fibroblasts annotated from two datasets were merged and further subclustered after batch correction using Seurat CCA. The fibroblast–T and fibroblast–endothelium doublet clusters were excluded for further analysis. Phenotype annotation was marker gene–based, as previously described (36), and downstream differential gene expression analysis was performed via model-based analysis of single-cell transcriptome with the FindMarkers function. Genes with a fold change >1.5 and an adjusted $P < 0.001$ were considered to be significantly upregulated. The REACTOME gene set enrichment analyses were performed using a hypergeometric test in the hypeR package (v1.9.1), and gene set overrepresentation was determined with a hypergeometric test.

Cell lines and cell culture

Human colorectal cancer cell line (SW480, CVCL_0546) was purchased from the ATCC. The cells in the experiment were all identified by short tandem repeat DNA profiling analysis and cultured within 20 to 30 generations, and there was no contamination of *Mycoplasma* or black gum worms.

Isolation of primary NFs and CAFs: Under sterile conditions, tumor tissues and corresponding normal intestinal tissues were collected from patients with colorectal cancer at the Sir Run Run Shaw Hospital, affiliated with Zhejiang University. Then, the tissues were minced and digested with collagenase IV (1 mg/mL, Gibco) and hyaluronidase (0.5 mg/mL, BioFroxx) for 1 hour at 37°C. The solution was centrifuged at 1,000 rpm for 5 minutes and washed twice with PBS. The supernatant was discarded, and 4 mL of DMEM containing 10% FBS (GIBCO) was added for resuspension. The solution was aspirated and sieved, and the filtrate was added to a 6 cm Petri dish. After the cells reached confluence, they were digested with trypsin for 2 minutes, centrifuged, and resuspended in a 6-cm dish. The medium was changed after 2 hours, and the fibroblasts (used within 10 generations) were purified by differential adhesion. The remaining undigested cells were digested. After observing only primary colorectal cancer cells under a microscope, TRIzol was utilized to collect RNA from the primary tumor cells for subsequent experiments.

Clinical samples

From October 2011 to August 2012, 180 paraffin-embedded specimens from patients with colorectal cancer confirmed by pathology who underwent surgical treatment at Sir Run Run Shaw Hospital were selected to make tissue microarrays (TMA). Fresh tumor tissue specimens and matched normal colon tissue specimens were obtained from 8 patients with colorectal cancer. The collected clinicopathologic data included sex, age, differentiation, the tumor–node–metastasis (TNM) stage, T stage, lymph node metastasis, distant metastasis, recurrence, and other clinicopathologic characteristics. The TNM stage of patients with colorectal cancer was based on the eighth edition of the American Joint Committee on Cancer staging system. Stool samples and matched tumor samples were collected in our previous study

(37). Multicolor staining was performed on the postoperative specimens of 9 patients with colorectal cancer, and the percentage of SULF1$^+$αSMA$^+$/αSMA$^+$ cells in the whole film was measured. According to the percentage of positive SULF1$^+$αSMA$^+$/αSMA$^+$ cells, the first three with the highest percentage of positive cells were defined as the high-expression group, the three with the lowest percentage of positive cells were defined as the low-expression group, and the rest are the medium expression group. We collected homologous recombination–positive, HER2-negative locally advanced or metastatic breast cancer tissues from patients who were treated with chidamide in combination with exemestane tablets. Each patient signed a written informed consent. Patients were reviewed every 3 months, and patients with reduced or stable metastasis were defined as the response group, whereas patients with progressive metastasis were defined as the nonresponse group. The study was conducted in accordance with ethical guidelines of Declaration of Helsinki. The ethics committees of Sir Run Run Shaw Hospital, Zhejiang University (20220209-256, 20220103-56), and the First Affiliated Hospital of Huzhou University (2021KYLL-Y005) had approved these studies.

FISH

Digoxin-labeled *SULF1* probes were designed and synthesized by Servicebio. The sequences used were h*SULF1*: TCAATGTATGCCTTATGGTCCTTCCACCGCTCT and mSulf1: CCCATAACTGTCCTCTGCGGGTCAGAG. The probe signals were determined using a FISH kit (RiboBio). The images were acquired under a fluorescence microscope (Nikon), and the fluorescence intensity was analyzed using ImageJ.

Immunofluorescence

Cell slides or tissue sections (after tissue dewaxing and antigen repair) were prepared. The cell membrane was broken with 0.5% Triton X 100 and blocked with 5% BSA, and the primary antibody was incubated at 4°C overnight. The antibodies included FSP1 (Proteintech, cat. #66489-1-Ig, RRID:AB_2881854), SULF1 (ATLAS, HPA054728), and CD31 (Proteintech, cat. #28083-1-AP, RRID:AB_2881055), and the second antibody was incubated. The slices were sealed using a DAPI sealing agent. Images were acquired by fluorescence microscopy (Nikon), and the fluorescence intensity was analyzed using ImageJ.

IHC staining

Paraffin sections were stained according to standard IHC staining methods. The primary antibodies used were SULF1 (ATLAS, HPA054728), Ki67 (Proteintech, cat. #27309-1-AP, RRID: AB_2756525), N-cadherin (Cell Signaling Technology, cat. #13116 (also 13116T and 13116S), RRID:AB_2687616), E-cadherin (Cell Signaling Technology, cat. #3195, RRID:AB_2291471), and CTHRC1 (Proteintech, 16534-1-AP). The IHC score adopts a 13-point method: 0 to 4 points to determine the percentage of stained positive cells; 0 points, no positive cells; 1 point, percentage of positive cells <10%; 2 points, percentage of positive cells 10% to 50%, 3 points, percentage of positive cells 50% to 80%; and 4 points, percentage of positive cells >80%. A score of 0 to 3 was used to evaluate the staining intensity, a score of 0 to 1 was considered negative, and a score of 2 to 3 was judged as positive. The final score is the product of the staining ratio and the staining intensity.

Commercial antibody microarray

Antibody microarray was Human Cytokine Antibody Array Q640 (catalog #GSH-CAA-64) purchased from RayBiotech. Antibody array provides a broader view of protein activity compared with single-target ELISA and Western blot. The array slides were treated and processed according to the manufacturer's instructions. The signals can be visualized using RayBio RPAS Microarray Scanner. Under the same conditions, the experiment was repeated four times for two groups of samples.

RNA extraction and quantitative RT-PCR

TRIzol reagent (Invitrogen) was used to extract total RNA from tissues and cell lines, and reverse transcription reagents (TaKaRa) were used to reverse-transcribe the total RNA into cDNA. Specific primers were used to detect the mRNA level of the target gene based on the abovementioned cDNA as the template. The primer sequences are listed in Supplementary Table S1.

Cell contraction assay

A total of 5×10^4 CAFs were mixed in 1 mg/mL type I rat tail collagen and added to a 24-well plate. After the gel solidified, DMEM containing 10% FBS was added to the gel, the gel contraction was monitored daily, and pictures were taken. Gel contraction values were calculated using ImageJ after 3 days.

Masson's trichrome staining

Tissue sections were cut to 4 μm and stained with a modified Masson trichrome solution (Solarbio). Briefly, sections were deparaffinized with xylene, rehydrated with graded ethanol, mordant overnight, lapis lazuli blue and Mayer hematoxylin staining, acid ethanol differentiation, Ponceau red fuchsin staining, aniline blue staining after phosphomolybdic acid solution treatment, and dehydration and mounting after weak acid neutralization.

RNA sequencing analysis

Surgical specimens from three cases of early colorectal cancer and three cases of colorectal cancer with distant metastasis were collected. Normal intestinal fibroblasts and tumor-associated fibroblasts were cultured in primary culture. RNA was collected using TRIzol, and transcriptome sequencing was performed at Meggie Bio-Company. To identify differentially expressed genes (DEG) between two different groups (Supplementary Materials S1), the expression level of each gene was calculated according to the transcripts per million reads method. RSEM (http://deweylab.biostat.wisc.edu/rsem/) was used to quantify gene abundances. Essentially, differential expression analysis was performed using DESeq2 with $|\log_2(\text{fold change})| \geq 1.2$ and P-adjust ≤0.001 were considered to be substantially different expressed genes. In addition, functional enrichment analysis including Gene Ontology (GO, http://www.geneontology.org) and Kyoto Encyclopedia of Genes and Genomes (KEGG; http://www.genome.jp/kegg/) analyses, were performed to identify DEGs that were significantly enriched in GO terms and metabolic pathways at P adjust ≤0.05, compared with the whole-transcriptome background. We performed RNA sequencing (RNA-seq) using the control or SULF1^{KD} CAFs through this method. The DEGs are shown in Supplementary Materials S2.

Multicolor staining

OPAL Assay Kits purchased from Akoya Biosciences were used for multicolor staining. We conducted the experiment according to OPAL multiplexing method. OPAL is based on tyramide signal

amplification. Tissue sections were stained with antibodies against, and the fluorescence signals were generated using the following fluorophores: OPAL 690/520/570/620/480 (Akoya Biosciences). Multiplex-stained slides were imaged using the PhenoImager Fusion Automated Quantitative Pathology Imaging System (Akoya Biosciences). For quantitative analysis, QuPath software was applied to quantify the cell density of nucleus area per cell, expression per cell and area per cell. For spatial analysis, the numbers of $CD31^+$ cells were quantified according to the distance gradients (0–25, 25–50, 50–100, 100–150, and 100–150 μm) from $SULF1^+\alpha SMA^+$ cells using QuPath software.

Protein extraction and Western blot analysis

Proteins from fresh tissues and cell lines were treated with RIPA buffer containing protease and phosphorylase inhibitors. The protein concentration was determined by the BCA method, and proteins were separated by 8% to 12% SDS-PAGE and transferred to polyvinyl difluoride membranes. The membranes were incubated overnight at 4°C, with the corresponding primary antibodies including SULF1 (Atlas Antibodies, cat. #HPA054728, RRID: AB_2682586), GAPDH (Cell Signaling Technology, cat. #5174, RRID:AB_10622025), VEGFA (Proteintech, cat. #19003-1-AP, RRID:AB_2212657), VEGFR2 (Abcam, cat. #ab134191, RRID: AB_2934135), P-PI3K (Cell Signaling Technology, cat. #4228, RRID:AB_659940), AKT (Cell Signaling Technology, cat. #4691, RRID:AB_915783), P-AKT308 (Cell Signaling Technology, cat. #13038, RRID:AB_2629447), P-AKT473 (Cell Signaling Technology, cat. #4060, RRID:AB_2315049), CREB1 (Proteintech, cat. #12208-1-AP, RRID:AB_2245417), P-CREB1 (Proteintech, cat. #28792-1-AP, RRID:AB_2918203), and CTHRC1 (Proteintech, cat. #16534-1-AP, RRID:AB_2087511).

Coimmunoprecipitation

The cells were collected in 10-cm plates, and 1 mL of IP Lysis (Thermo Fisher Scientific, 1861603) containing protease inhibitor and phosphorylase inhibitor was added. The plates were incubated with an antibody at 4°C overnight, magnetic beads were added the next day, the plates were incubated for 4 hours, the mixture was centrifuged and washed, 5× protein loading was added, the eluate product was finally heated, and the level of the target protein was detected via Western blotting.

Dual-luciferase reporter assay

The CREB1-pcDNA3.1 plasmid, CTHRC1 promoter region-PGL3 plasmid, and *Renilla* luciferase plasmid were constructed. The plasmids of different groups were transferred into 293T cells (CVCL_0063). After 24 hours, the fluorescence intensities of firefly luciferase and *Renilla* luciferase were detected using a dual-luciferase reporter test kit (Yeasen, 11402ES60). The ratio of firefly luciferase intensity to *Renilla* luciferase intensity was used to display the activation of the CTHRC1 promoter region.

Chromatin immunoprecipitation

Cells were collected in 15-cm plates, and a chromatin immunoprecipitation kit (Millipore, 17-295) was used for cross-linking and splitting according to the manufacturer's protocol. The antibodies were added, the protein–DNA complex was eluted, the DNA was purified, primers were used to amplify the product, and electrophoresis was conducted on an agar gel.

High-throughput 16S ribosomal RNA gene sequencing

The genomic DNA from the stool of 17 patients with colorectal cancer was extracted using TGuide S96 Magnetic Stool DNA Kit (TIANGEN Biotech) according to the manufacturer's instructions. The V1–V9 hypervariable regions of the 16S rRNA gene were amplified using primers (27F: AGRGTTTGATYNTGGCTCAG; 1492R: TASGGHTACCTTGTTASGACTT). The amplicons were quantified, after which, the normalized equimolar concentrations of amplicons were pooled and sequenced on the PacBio Sequel II platform (Beijing Biomarker Technologies).

Tube formation assay

The wells of a 24-well plate were coated with 300 μL/well Matrigel (BD Biosciences). Human umbilical vein endothelial cells (HUVEC; CVCL_2959; 2×10^5/well) were then added to the precoated wells in 500 μL of CAF-CM and cultured for 8 to 12 hours. The plates were observed and photographed using an inverted microscope, and ImageJ software was used to enumerate the complete tubular structures.

Animal studies

Fibroblasts and mCherry fluorescence-transfected SW480 cells were used for tumorigenesis in nude mice (subcutaneous transplantation for 21 days, lung and liver metastasis models of colorectal cancer for 21–30 days) at a 1:5 ratio, 2×10^6 SW480 and 4×10^5 fibroblasts for subcutaneous transplantation, 10^6 SW480 and 2×10^5 fibroblasts for lung and liver metastasis models. Four-week-old female nude mice were selected to observe the tumor size and animal model indicators, hematoxylin and eosin (H&E) staining, and IHC staining. At the same time, we constructed the models of luci-transfected SW480 and mCherry-transfected fibroblasts coinjected into nude mice for subcutaneous, lung metastasis and liver metastasis, and the presence of fibroblasts during model construction was demonstrated by *in vivo* imaging and immunofluorescence (IF) staining of tissues. Purchase $Sulf1^{flox/+}$mice (Cyagen) were mated with *Col1a2-CreER* mice to produce *Col1a2-CreER;* $Sulf1^{flox/flox}$ is a fibroblast-specific Sulf1 knockout mouse ($Sulf1^F$ KO), and *Col1a2-CreER*; $Sulf1^{+/+}$ is the control group ($Sulf1^F$ WT). After induction with tamoxifen, we performed 10^6 transfected MC38 (CVCL_B288) cells in two groups of mice subcutaneous, subserosal cecum (38), or tail vein. Twenty-one days later, 150 mg/kg D-fluorescein (Yeasen) was injected intraperitoneally. Ten minutes later, the mice were anesthetized with isoflurane, and the tumor cells labeled with light were imaged using IVIS (PerkinElmer). The tumor size and animal model indicators were observed, and H&E staining and IHC staining were performed. The study was approved by the Ethics Committee of the Sir Run Run Shaw Hospital, Zhejiang University (SRRSH202202309).

Statistical analysis

The data are expressed as the mean ± SD. Group comparisons were performed using paired or unpaired two-tailed Student *t* tests and one-way ANOVA followed by Bonferroni correction. χ^2 tests or one-way ANOVA were used to evaluate the associations between the SULF1 expression and the clinicopathologic features of patients with colorectal cancer in the TMA. The Kaplan–Meier analysis was used to evaluate the effect of SULF1 on overall survival (OS) in patients with colorectal cancer with TAM. The correlation between SULF1 and various SCFAs in colorectal cancer tissues was determined by Spearman correlation analysis. The SPSS software and GraphPad Prism 8 software were used for statistical analysis, and

the statistical significance was set to *, $P < 0.05$; **, $P < 0.01$; and ***, $P < 0.001$.

Data availability

The RNA-seq data have been uploaded to the SRA database at accession number PRJNA1126150 and PRJNA1127019. The data of 16S ribosomal RNA gene sequencing have been uploaded to the SRA database at accession number PRJNA1126386. The data analyzed in this study were obtained from Gene Expression Omnibus at GSE144735 (https://www.ncbi.nlm.nih.gov/geo/query/acc.cgi?acc=GSE144735) and GSE132465 (https://www.ncbi.nlm.nih.gov/geo/query/acc.cgi?acc=GSE132465). All other raw data are available upon request from the corresponding author.

Results

Single-cell sequencing identifies SULF1$^+$ CAFs in colorectal cancer

First, we analyzed a total of 51 samples including tumor tissue (core and border) and paired normal tissue from 29 patients with colorectal cancer using publicly available single-cell sequencing datasets (datasets GSE132465 and GSE144735; ref. 39). The major cell clusters are shown in Supplementary Fig. S1A and S1B. To further investigate the heterogeneity of fibroblasts, we performed subclustering analysis and identified a total of 10 fibroblast-related cell subtypes (**Fig. 1A**). The marker genes for these subtypes were identified separately (**Fig. 1B** and **C**). Most of these cell subtypes are consistent with the findings of Lee and colleagues (39) and Qian and colleagues (36), but this study revealed more CAF subtype (**Fig. 1D**). We identified a total of five subtypes (CAF1–CAF5), which were enriched in the colorectal cancer tissues, particularly in tumor core, as compared with normal tissues. Among these subtypes, CAF1, CAF2, and CAF5 were newly identified subtypes, whereas their numbers were relatively small in tumors (**Fig. 1E**). The most abundant CAF subtype is the CAF3 (C5_SULF1), characterized by the high expression of marker genes such as *COMP* and *SULF1* (**Fig. 1B** and **C**). Through KEGG and Reactome enrichment analysis, we found that C5_SULF1 exhibited notably enhanced ECM, collagen signaling, and TGFβ signaling compared with other CAFs (**Fig. 1F** and **G**), suggesting a myofibroblastic phenotype *in silico*. Compared with other fibroblast subtypes in tumor tissues, the genes highly expressed in C5_SULF1 were mostly related to the ECM (*CTHRC1* and *BGN*) and collagen components (*COL1A1* and *COL3A1*; **Fig. 1H**; Supplementary Fig. S1C). In contrast to COMP and TGFβ whose regulatory roles have been extensively studied, the functions of SULF1 in CAFs are still unclear. Notably, high *SULF1* expression was specifically found in fibroblast compartment (**Fig. 1I**), whereas tumor cells, immune cells, and endothelial cells expressed lower levels of *SULF1*. In addition, *SULF1* expression in tumor tissues was dramatically greater than that in adjacent normal tissues (**Fig. 1J**). Hence, these results suggest that SULF1$^+$ CAFs may play a role in the regulation of colorectal cancer progression.

SULF1$^+$ CAFs predict poor prognosis in colorectal cancer

To gain a deeper understanding of the clinical relevance of SULF1 in patients with colorectal cancers, we collected primary normal fibroblasts (NF) and the matched CAFs from patients with colorectal cancer, qPCR results showed that *SULF1* expression was markedly increased in CAFs compared with NFs (**Fig. 2A**; Supplementary Fig. S2A). In contrast to CAFs, the matched primary colorectal cancer cells expressed extremely low levels of *SULF1* (**Fig. 2B**). Four of the 8 patients were randomly selected for the analysis of SULF1 protein expression by Western blotting, and the results confirmed that SULF1 expression was higher in CAFs than in NFs (Supplementary Fig. S2B). Through performing *in situ* hybridization (ISH), we found that *SULF1* expression was significantly higher in the interstitium of colorectal cancer tissues than that in the adjacent normal tissues (**Fig. 2C**). FISH assay further showed that *SULF1* was colocalized with *FSP1*, a fibroblast marker gene (**Fig. 2D**). The colocalization between SULF1 and FSP1 was further validated at the protein level through IF staining (**Fig. 2E**).

To explore the prognostic significance of SULF1, FISH and IF staining were conducted using TMA containing 180 colorectal cancer tissues (**Fig. 2F**). χ^2 analysis showed that high expression of protein of SULF1 in the interstitium of colorectal cancer was associated with high TNM staging, T staging, and high likelihood of metastasis and recurrence (Supplementary Table S2). It was shown that the TNM stage was correlated positively with the proportion of high SULF1 expression (**Fig. 2G**). Multiple regression analysis revealed that high expression of SULF1 protein was an independent risk predictor of poor prognosis of colorectal cancer (Supplementary Table S3). Importantly, the expression of protein of SULF1 was significantly negatively correlated with the OS of patients with colorectal cancer (**Fig. 2H**). Consistently, in The Cancer Genome Atlas (TCGA) datasets, patients with colorectal cancer with high *SULF1* expression had a significantly poorer prognosis than those with low *SULF1* expression (Supplementary Fig. S2C and S2D). We then conducted RNA-seq of paired NFs and CAFs from 6 patients with colorectal cancer with or without distant metastasis and found that *SULF1* expression was markedly increased in metastatic CAFs compared with that in nonmetastatic CAFs (**Fig. 2I**). Strikingly, *SULF1* is the most robustly upregulated gene in CAFs compared with NFs in patients with metastatic (Supplementary Fig. S2E). The highest *SULF1* expression was observed in the poor-prognosis stroma-rich molecular subtype of colorectal cancer [consensus molecular subtype 4 (CMS4); **Fig. 2J**]. Taken together, these results indicate that high SULF1 expression in CAFs is associated with poor patient outcome in colorectal cancer.

SULF1$^+$ CAFs facilitate the malignant behaviors of colorectal cancer

To further investigate the effects of SULF1$^+$ CAFs on colorectal cancer progression, we generated tamoxifen-induced, fibroblast-specific Sulf1 knockout mice (*COL1A2-CreER; Sulf1$^{fl/fl}$*, Sulf1^F-KO; **Fig. 3A**; Supplementary Fig. S3A) and inoculated these mice with murine MC38 colorectal cancer cells expressing luciferase. As shown in **Fig. 3B** and **C**, Sulf1 deficiency in fibroblasts significantly inhibited tumor growth. The numbers of Sulf1$^+$ and Ki67$^+$ cells were significantly decreased in KO group (**Fig. 3D**). Furthermore, we injected MC38 cells *in situ* into the subserosa of cecum of mice to construct an orthotopic model. The results showed that fibroblast-specific Sulf1 knockout inhibited the ability of MC38 cells to form tumors *in situ* (**Fig. 3E**; Supplementary Fig. S3B) and the numbers of Ki67$^+$ cells were significantly decreased in KO group (**Fig. 3F**). Epithelial–mesenchymal transition is the process of transforming epithelial cells into mesenchymal phenotypes, accompanied by an increase in cell motility and the expression or function of epithelial genes such as E-cadherin is lost during the transition, whereas the expression of genes that define the mesenchymal phenotype, such as N-cadherin is elevated (40, 41). To detect effects of SULF1$^+$ CAFs on tumor metastasis, we used fibroblast-specific Sulf1 knockout mice, MC38 colorectal cancer cells expressing luciferase were

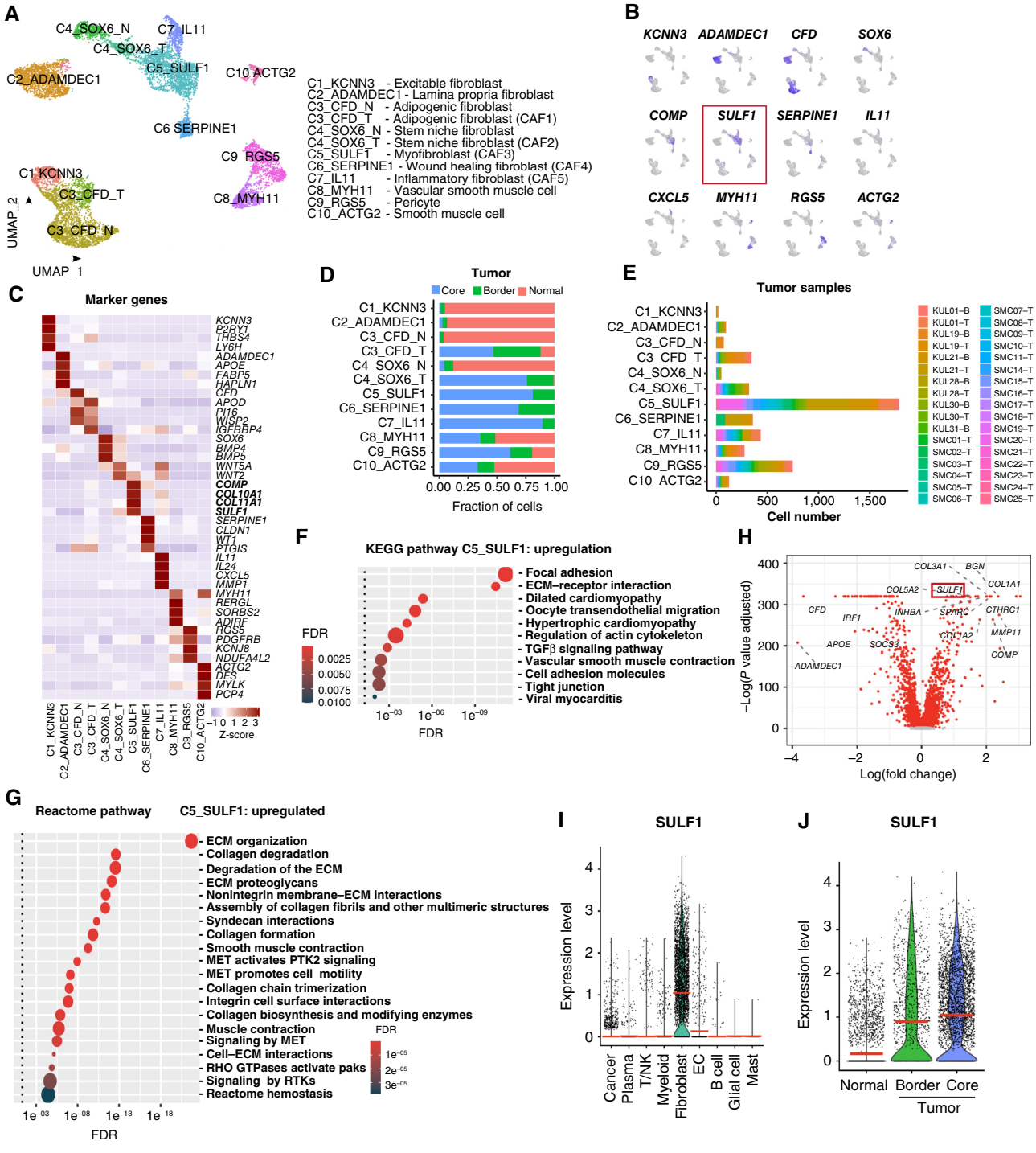

Figure 1.

Single-cell sequencing identifies SULF1$^+$ CAFs in colorectal cancer. **A,** Ten subtypes were found in the form of Uniform Manifold Approximation and Projection (UMAP) following dimension reduction, clustering, and identification of 9,381 colorectal cancer fibroblast single-cell transcriptome data. **B,** UMAP map shows the expression level of representative marker genes of fibroblast-related subpopulations. **C,** Heatmap shows the expression level of representative marker genes of fibroblast-related subsets. **D,** Histogram statistics of the source and corresponding proportion of each fibroblast subtype. **E,** A histogram was used to calculate the sample source and corresponding cell number of each fibroblast subtype. **F,** Upregulated signaling pathway corresponding to the upregulated DEGs in CAF3 (C5_SULF1; KEGG database). **G,** Upregulated signaling pathway corresponding to the upregulated DEGs in CAF3 (C5_SULF1; REACTOME database). **H,** Differential gene analysis of CAF3 (C5_SULF1) and other fibroblast subpopulations in the tumor volcano map. Red dots, significantly changed genes, including significantly upregulated *SULF1*. **I,** *SULF1* is specifically upregulated in fibroblasts. **J,** *SULF1* is upregulated in tumors compared with normal adjacent tissues, and the upregulation rate in the core region of tumors was higher than that in the marginal region.

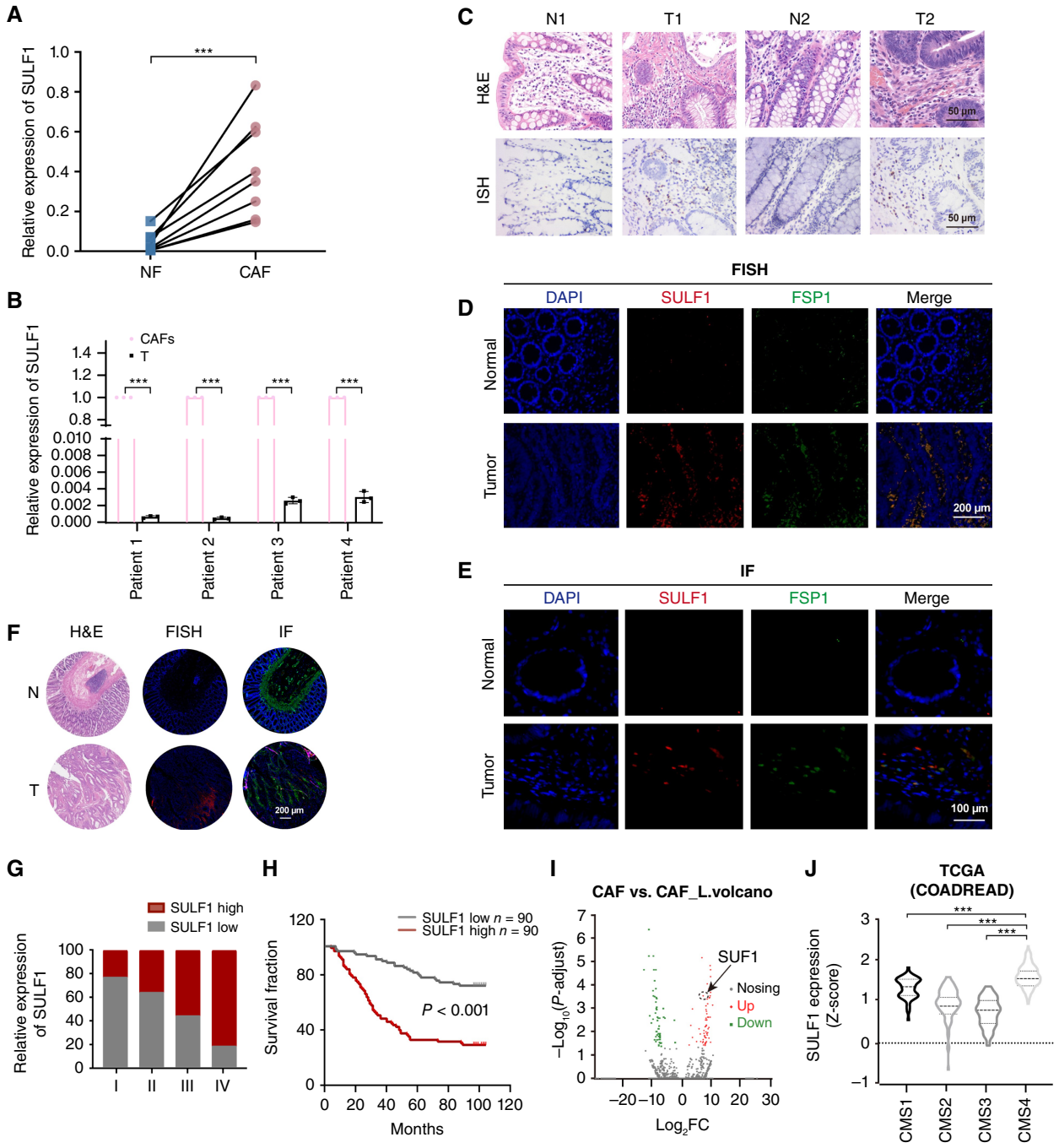

Figure 2.

SULF1+ CAFs predict poor prognosis in colorectal cancer. **A,** qPCR was used to verify the level of *SULF1* in NFs and their corresponding CAFs ($n = 8$). **B,** Level of *SULF1* in primary colorectal cancer cells and corresponding CAFs was verified by qPCR ($n = 4$). **C,** ISH was used to detect the expression of *SULF1* in tumor and normal tissues of colorectal cancer. Scale bar, 50 μm. **D,** FISH of the *SULF1* probe (red) and *FSP1* probe (green) to detect the costaining of *SULF1* and *FSP1* (yellow). Scale bar, 200 μm. **E,** The costaining (yellow) of SULF1 and FSP1 was detected by IF staining with SULF1 (red) and FSP1 (green). Scale bar, 100 μm. **F,** Fluorescence images of SULF1 in colorectal cancer TMA, as evaluated by FISH and IF. Red, SULF1; green, αSMA. Scale bar, 200 μm. **G,** The percentage of high/low expression of protein of SULF1 in patients with colorectal cancer of different tumor–node–metastasis stages. **H,** The OS of 180 patients with colorectal cancer in the TMA according to the protein levels of SULF1, as calculated by the Kaplan–Meier analysis. **I,** Volcano plot of the DEGs identified by transcriptome sequencing in CAFs from three patients with colorectal cancer with and three patients with colorectal cancer without metastasis. **J,** Expression level of *SULF1* in different colorectal cancer molecular types (CMS1, CMS2, CMS3, and CMS4) in TCGA database. The data are presented as the mean ± SD of three independent experiments, two-tailed Student *t* tests. ***, $P < 0.001$.

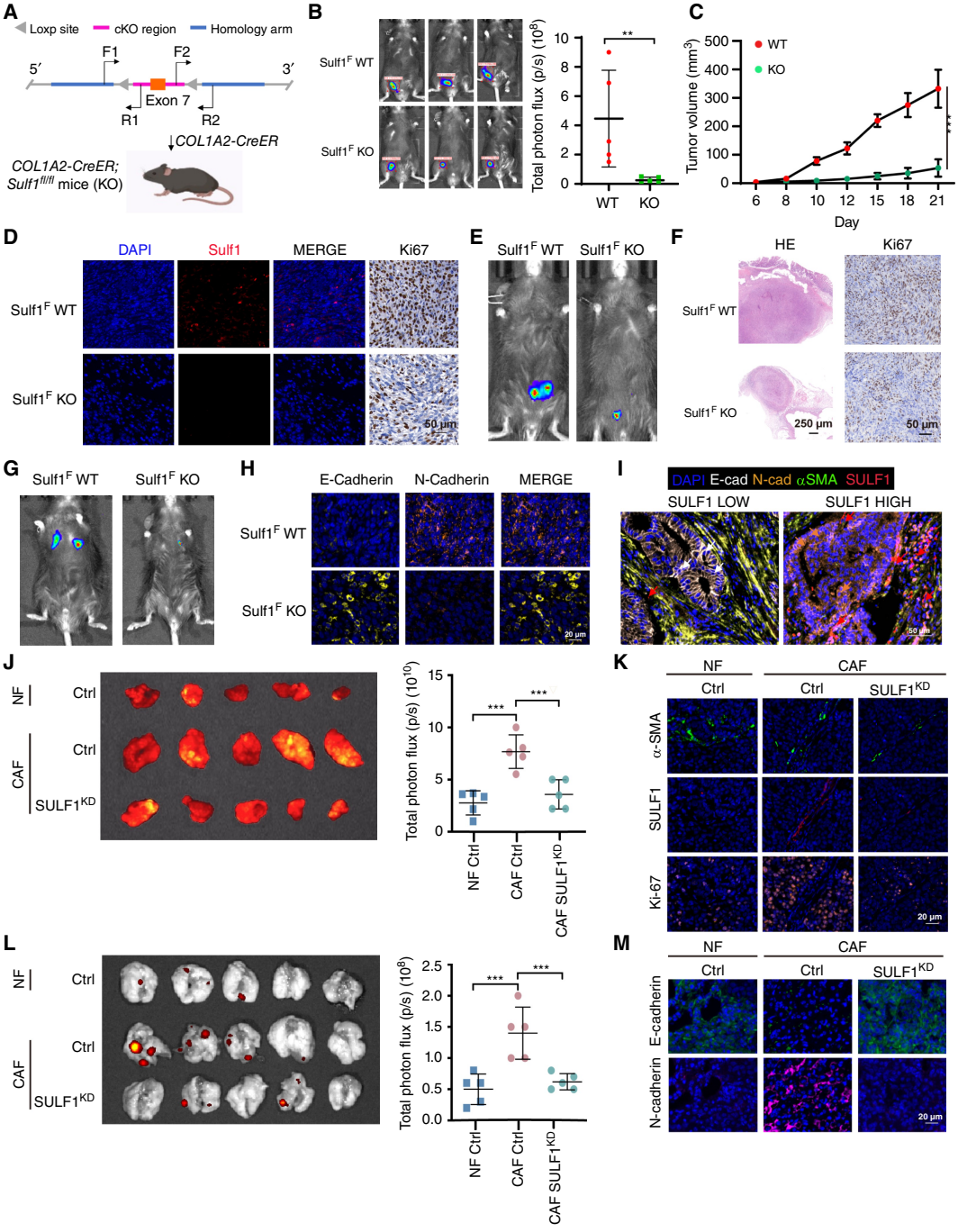

Figure 3.

SULF1^{+} CAFs facilitate the malignant behavior of colorectal cancer. **A,** Schematic of the construction and mating of *COL1A2-CreER; Sulf1$^{fl/fl}$* mice. **B,** Changes in the fluorescence intensity of subcutaneous tumors in the two groups. **C,** Tumor volume in the two groups. **D,** H&E, IF of the Sulf1, and IHC staining of Ki67 in the two groups. Scale bar, 50 μm. **E,** Changes in the fluorescence intensity of the orthotopic model in the two groups ($n = 3$). **F,** H&E and IHC staining of Ki67 in the two groups. Scale bar, 250, 50 μm. **G,** Changes in the fluorescence intensity of lung metastasis in the two groups ($n = 3$). **H,** IF of E-cadherin and N-cadherin in the two groups. Scale bar, 20 μm. **I,** Multicolor staining of patients with colorectal cancer with low- and high-expression SULF1. Scale bar, 50 μm. **J,** SW480 and NF Ctrl, CAF Ctrl, CAF SULF1^{KD} cells were implanted subcutaneously into nude mice at a ratio of 5:1 to verify the effects of different groups on the subcutaneous tumorigenesis of SW480 cells and the change of fluorescence intensity in subcutaneous tumors in the three groups ($n = 5$). **K,** Difference in the IF of SULF1 level and Ki67-positive rate among the three groups. Scale bar, 20 μm. **L,** SW480 and NF Ctrl, CAF Ctrl, CAF SULF1^{KD} were injected into the tail vein of nude mice at a ratio of 5:1 to verify the effects of different groups on lung metastasis of SW480 and the change in fluorescence intensity of pulmonary metastatic tumor in the three groups ($n = 5$). **M,** IF staining of three groups of lung metastatic tumors with E-cadherin and N-cadherin. Scale bar, 20 μm. The data are presented as the mean ± SD of three independent experiments, two-tailed Student *t* tests. **, $P < 0.01$; ***, $P < 0.001$.

injected into tail vein of the mice. The results showed that Sulf1 deficiency in fibroblasts significantly inhibited lung metastasis (**Fig. 3G**; Supplementary Fig. S3C and S3D). In addition, decreased N-cadherin and increased E-cadherin were observed in KO group (**Fig. 3H**). Multicolor staining using patients with colorectal cancer and elevated levels of SULF1 expression also demonstrated that higher SULF1 expression was accompanied by increased N-cadherin expression and decreased E-cadherin expression (**Fig. 3I**).

We then knocked down SULF1 expression in human primary CAFs (Supplementary Fig. S3E) and coinjected mCherry-labeled SW480 colorectal cancer cells with NFs, CAFs, or SULF1^{KD} CAFs into nude mice. The results showed that CAFs significantly accelerated the progression of SW480 tumors compared with NFs. Importantly, SULF1 knockdown significantly compromised the protumor capacity of CAFs (**Fig. 3J**; Supplementary Fig. S3F and S3G). In addition, the expression of Ki67 was significantly decreased in SW480 tumors coinjected with SULF1^{KD} CAFs (**Fig. 3K**).

To detect the influence of SULF1$^+$ CAFs on tumor cellular motility, we established two colorectal cancer metastasis models via coinjecting SW480 cells and fibroblasts into the tail vein and spleen of nude mice. The results showed that the number and size of lung and liver metastatic nodules were significantly reduced by SULF1 knockdown in CAFs (**Fig. 3L**; Supplementary Fig. S3H–S3L). In addition, decreased N-cadherin with increased E-cadherin was observed when SULF1 expression was silenced in CAFs, suggesting that SULF1 expression in CAFs affected the epithelial–mesenchymal transition progression of colorectal cancer cells (**Fig. 3M**; Supplementary Fig. S3M). These results indicate that SULF1$^+$ CAFs promote growth and metastasis of colorectal cancer.

To demonstrate the presence of fibroblasts in the subcutaneous coinjection model, we transfected SW480 cells with luciferase and fibroblasts with mCherry. Twenty-one days later, the tissue of mice subcutaneous tumor was collected, and IF staining was performed to demonstrate the persistent presence of coinjected fibroblasts in the subcutaneous tumor tissue (Supplementary Fig. S4A). Strikingly, coinjecting fibroblasts-mCherry with SW480-luci was detected in the metastases (Supplementary Fig. S4B–S4E).

SULF1$^+$ CAFs promotes tumor angiogenesis in a VEGFA-dependent manner

To explore the mechanisms of SULF1-mediated tumor progression, we performed GSH-CAA640 protein array to detect the differentially expressed proteins in the supernatant of Ctrl CAFs and SULF1^{KD} CAFs (**Fig. 4A**). The STRING database was used to construct a protein–protein interaction network, which showed key downregulated differentially expressed proteins such as IL6 and VEGFA (**Fig. 4B**). Through applying MCC algorithms, IL6, VEGFA, SERPINE1, SPP1, and HGF were identified as top five hub proteins (Supplementary Fig. S5A). SULF1 is known to alter the sulfide state of HSPG to regulate the bioavailability of multiple HS-binding proteins (42, 43). Among these proteins, we found that the knockdown of SULF1 reduced the level of VEGFA in the supernatant (**Fig. 4C**). ELISA experiments showed that SULF1 knockdown reduced the level of VEGFA in CAF supernatant. However, the mRNA levels of *VEGFA* remained unchanged in SULF1^{KD} CAFs (Supplementary Fig. S5B and S5C).Gene set enrichment analysis revealed that SULF1^{KD} was significantly anticorrelated with angiogenesis (**Fig. 4D**). Multicolor staining determined the knockout efficiency of Sulf1 in Sulf1^F-KO mice (Supplementary Fig. S5D). For further spatial analysis, we quantified the number of CD31$^+$ cells within the distance gradients (0–20, 20–40 μm) of Sulf1$^+$αSMA $^+$CAFs in the tumor tissues of Sulf1^F WT and Sulf1^F-KO mice. As expected, over a range of distance from Sulf1$^+$αSMA$^+$ CAFs, the number of CD31$^+$ cells showed a decreasing trend after specific knockout of Sulf1 in CAFs (**Fig. 4E**), indicating the crucial role of SULF1$^+$ CAFs in facilitating tumor angiogenesis. Multicolor staining using patients with colorectal cancer with elevated levels of the ratio of SULF1$^+$αSMA$^+$/αSMA$^+$ also demonstrated that over a range of distance (0–25, 25–50 μm) from SULF1$^+$αSMA$^+$CAFs, the number of CD31$^+$ cells showed an increasing trend (**Fig. 4F**; Supplementary Fig. S5E). In SULF1 high-expression group, it was shown that the greater the distance (0–25, 25–50, 50–100, 100–150, and 150–200 μm) from SULF1$^+$αSMA $^+$ cells, the CD31$^+$cells showed a decreasing trend (**Fig. 4F**), which confirmed the spatially close relationship between SULF1$^+$ CAFs and CD31$^+$cells. Furthermore, multicolor staining revealed that SULF1$^+$ CAFs were in closer proximity to CD31$^+$ than SULF1$^-$ CAFs (Supplementary Fig. S5F).

In *in vitro* experiments, we cultured HUVEC with the conditional medium (CM) from CAFs and found that the tube formation capacity of HUVECs cultured with CM from control CAFs was significantly impaired by a VEGFA-neutralizing antibody. In contrast, HUVECs cultured with CM from SULF1^{KD} CAFs showed an impaired capacity to induce tube formation of HUVECs, and this effect was not further reduced by VEGFA neutralization (**Fig. 4G**), suggesting that CAF-expressed SULF1 facilitates angiogenic ability of endothelial cells in a VEGFA-dependent manner. In colorectal cancer mice, VEGFA neutralization reduced tumor growth (**Fig. 4H**; Supplementary Fig. S5G) in mice coinjected with WT CAFs but not those with SULF1^{KD} CAFs. In addition, CD31 staining was also decreased as the tumor growth reduction (**Fig. 4I**). These results indicate that SULF1$^+$ CAFs promote tumor angiogenesis in a VEGFA-dependent manner.

SULF1$^+$ CAFs positively regulate ECM deposition in a VEGFA-dependent manner

To further dissect the effect of SULF1 in CAFs, we performed RNA-seq using control or SULF1^{KD} CAFs. GO analysis revealed that genes downregulated in SULF1^{KD} CAFs were enriched mainly in pathways related to the chemotaxis of immune cells, the regulation of cell adhesion, and the composition of ECM components, which is consistent with the results of our single-cell sequencing data (**Figs. 1G** and **H**, **5A**). Cell contraction assays and wound-healing assays showed that SULF1 knockdown inhibited the contraction and migration abilities of CAFs (**Fig. 5B**; Supplementary Fig. S6A). In colorectal cancer mice, SULF1 knockdown in CAFs decreased collagen components as evidenced by Masson staining (**Fig. 5C**). Consistently, collagen components were also reduced in Sulf1^F-KO mice compared with Sulf1^F WT mice (**Fig. 5D**).

Next, we clustered matrix-associated proteins detected by RNA-seq and intersected them with matrix proteins in CAFs detected by single-cell sequencing. The analysis revealed nine target genes that are potentially regulated by SULF1 in CAFs (**Fig. 5E**; Supplementary Fig. S6B). In addition, the expression of these nine genes was significantly positively correlated with *SULF1* expression in TCGA colorectal cancer cohorts (Supplementary Fig. S6C). Among these nine genes, *CTHRC1* was the second most differentially expressed gene between NFs and CAFs (Supplementary Fig. S2A), and exhibited the most robust downregulation in response to *SULF1* deletion in CAFs (Supplementary Fig. S6D), indicating that CTHRC1 is a target gene of SULF1. Similar to the expression profile of *SULF1*, the highest *CTHRC1* expression was observed in the

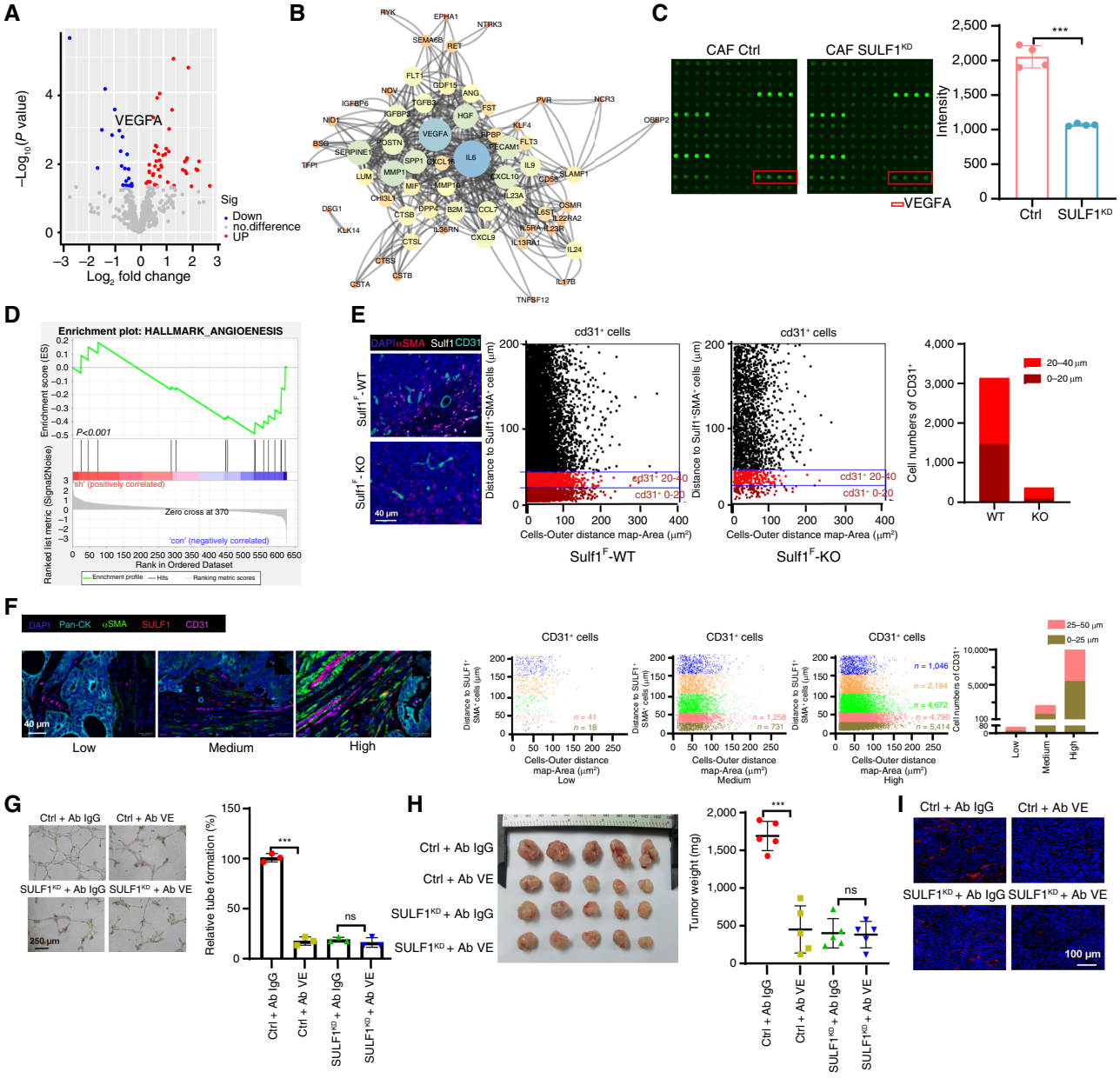

Figure 4.

SULF1$^+$ CAFs promote tumor angiogenesis in a VEGFA-dependent manner. **A,** Volcanic maps of different proteins in the supernatants of CAFs and CAF SULF1^{KD}. **B,** Protein–protein interaction network of different proteins in the two groups. **C,** Expression of VEGFA in the supernatants of the two groups. **D,** Gene set enrichment analysis of genes associated with angiogenesis. **E,** Multicolor staining of Sulf1^F WT and Sulf1^F KO. Scale bar, 40 μm. **F,** Multicolor staining of patients with colorectal cancer with different levels of the ratio of SULF1$^+$αSMA$^+$ to αSMA$^+$. Scale bar, 40 μm. **G,** Tube formation was evaluated in HUVECs cultured for 8 hours in medium collected from CAFs treated as described. **H,** SW480 and CAF Ctrl, CAF SULF1^{KD} cells were implanted subcutaneously into nude mice treated with VEGFA or IgG neutralization (150 μg, i.p. twice a week). **I,** IF staining of CD31 in the four groups. Scale bar, 100 μm. The data are presented as the mean ± SD of three independent experiments, two-tailed Student *t* tests. ns, nonsignificant; ***, $P < 0.001$.

poor-prognosis stroma-rich molecular subtype of colorectal cancer (CMS4), and single-cell analysis showed that the expression levels of *SULF1* and *CTHRC1* were consistent in different fibroblast subtypes (Supplementary Fig. S6E and S6F).

To determine the mechanism underling SULF1-mediated CTHRC1 expression in CAFs, we performed KEGG analysis, and found that *SULF1* knockdown altered gene expression in many signaling pathways, and the PI3K/AKT signaling pathway was the most overrepresented with 26 related genes (**Fig. 5F**). Consistently, knockdown of SULF1 in CAFs inhibited the activation of PI3K-AKT signaling pathway and reduced the expression of CTHRC1 (**Fig. 5G**; Supplementary Fig. S6G). In addition, treatment with

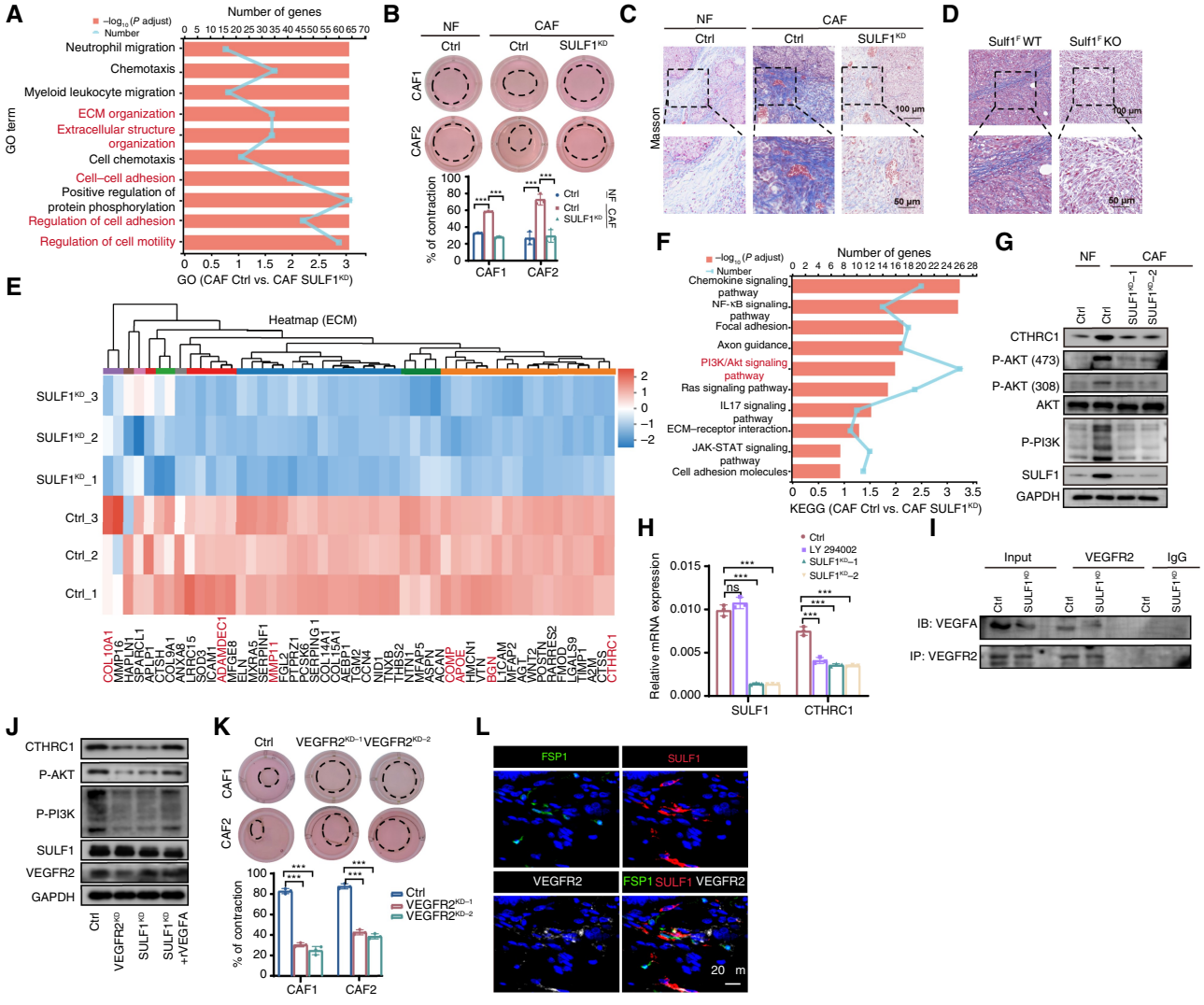

Figure 5.

SULF1+ CAFs enhance ECM deposition in a VEGFA-dependent manner. **A,** Gene Ontology (GO) functional enrichment showed that cell functions were affected mainly by the knockdown of SULF1 in CAFs. **B,** Cell contraction assay to verify the effect of SULF1 knockdown in CAFs on CAF contractility. **C,** Masson trichrome staining to verify the effect of SULF1 knockdown in CAFs on the production of extracellular collagen. Scale bar, 50 μm. **D,** Masson trichrome staining to verify the effect of conditional Sulf1 knockout in CAFs on the production of extracellular collagen. Scale bar, 50 μm. **E,** Heatmap showing ECM proteins affected by knockdown of SULF1 in CAFs. **F,** KEGG pathway enrichment analysis showed that cell function was mainly affected by SULF1 knockdown in CAFs. **G,** Western blotting detected the effect of SULF1 knockdown in CAFs on the PI3K/AKT signaling pathway and the protein level of CTHRC1. **H,** qPCR to verify the mRNA level of *CTHRC1* with the addition of the PI3K inhibitor LY294002 or knockdown of SULF1 in CAFs. **I,** Coimmunoprecipitation experiment to verify the combination of VEGFR2 and VEGFA after knockdown of SULF1 in CAFs. **J,** The protein levels of PI3K/AKT signaling pathway and CTHRC1 in the four groups were detected by Western blotting. **K,** Cell contraction assay to verify the effect of VEGFR2 knockdown in CAFs on CAF contractility. **L,** IF staining of FSP1(green), SULF1 (red), and VEGFR2 (white). Scale bar, 20 μm. The data are presented as the mean ± SD of three independent experiments, two-tailed Student *t* tests. ns, nonsignificant; **, $P < 0.01$; ***, $P < 0.001$.

PI3K inhibitor LY294002 significantly inhibited the expression of *CTHRC1* in CAFs (**Fig. 5H**). These results indicate that SULF1 promotes CTHRC1 expression in a PI3K/AKT-dependent manner.

Next, we explored how SULF1 affects the PI3K/AKT signaling pathway in CAFs. It was found that the knockdown of SULF1 reduced the level of VEGFA in the supernatant, which was a known upstream molecule of PI3K/AKT signaling pathway (**Fig. 4C**). Coimmunoprecipitation experiment showed that the knockdown of SULF1 in CAFs prevented the binding of VEGFA to VEGFR2 (**Fig. 5I**), suggesting that SULF1 affects the VEGFA chelation capacity by HSPG. Knockdown of VEGFR2 or SULF1 inhibited the activation of PI3K and AKT signaling pathway and decreased CTHRC1 expression in CAFs. Treatment of SULF1-depleted CAFs with recombinant VEGFA reversed the changes in the activation of PI3K/AKT signaling and the expression of CTHRC1 (**Fig. 5J**). Cell contraction assays also showed that VEGFR2 knockdown inhibited

the contraction ability of CAFs (**Fig. 5K**), indicating that SULF1$^+$ CAFs regulate ECM deposition by increasing the bioavailability of VEGFA. In addition, the expression of *KDR* was significantly positively correlated with *SULF1* expression in TCGA colorectal cancer cohorts (Supplementary Fig. S6H), and in the clinical samples of colorectal cancer and in colorectal cancer clinical samples, we detected VEGFR2 expression in SULF1$^+$ CAFs in the interstitium (**Fig. 5L**).

Using the Jaspar website, we predicted that transcription factors FOXO1 and CREB1 downstream from the PI3K/AKT pathway bind to the promoter region of CTHRC1 (Supplementary Materials), and further knockdown of *FOXO1* and *CREB1* in CAFs to detect the mRNA level of *CTHRC1* showed that depletion of *CREB1* reduced mRNA level of *CTHRC1*, whereas knocking down *FOXO1* had no effect on the mRNA level of *CTHRC1*, so CREB1 may potentially regulate the transcription of *CTHRC1* (Supplementary Fig. S7A). Immunoblotting analyses showed that CREB1 depletion inhibited the expression of CTHRC1 in CAFs, and protein detection in the extracted supernatant showed that CREB1 depletion reduced the protein level of CTHRC1 in culture supernatant (Supplementary Fig. S7B). Luciferase reporter analyses showed that CREB1 expression enhanced the luciferase activity driven by CTHRC1 promoter (Supplementary Fig. S7C). Consistently, analyses of CTHRC1 promoter regions predicted that CREB1 binds to the 472-691 region, which was validated by the chromatin immunoprecipitation assay using a CREB1 antibody (Supplementary Fig. S7D). Immunoblotting analyses found that SULF1 depletion or LY294002 treatment reduced the levels of phosphorylated (P)-PI3K, P-AKT, P-CREB1, and CTHRC1 in CAFs, and the level of CTHRC1 in culture supernatant (Supplementary Fig. S7E), and cell contraction assays demonstrated that SULF1 depletion, LY294002 treatment, and CTHRC1 depletion inhibited the contraction ability of CAFs (Supplementary Fig. S7F). These results indicate that SULF1 regulates the CTHRC1 expression via the VEGFA–PI3K–CREB1 axis.

SULF1 upregulation in CAFs is attributed to low butyrate production

The enhanced SULF1 expression in CAFs prompted us to look at the mechanisms contributing to SULF1 upregulation. Culture of CAFs with CM from colorectal cancer cells failed to increase *SULF1* expression in CAFs (**Fig. 6A**). It is known that gut microbial metabolites have profound impacts on tumor growth (44). Interestingly, when we treated CAFs with fecal extracts from patients with colorectal cancer, *SULF1* expression was significantly increased compared with CAFs treated with fecal extracts from healthy subjects (**Fig. 6B**), indicating a possible role of gut microbial metabolites in the modulation of SULF1 expression. Given that SCFAs are the most abundant metabolites in the mammalian colon (28), we examined the levels of four major SCFAs, including acetate, propionate, butyrate, and pentanoate, which were significantly reduced in the feces from patients with colorectal cancer compared with those from healthy subjects in our previous study (37). Among these SCFAs, only butyrate significantly inhibited SULF1 expression in CAFs at mRNA and protein levels in a dose- and time-dependent manner (**Fig. 6C–E**). Consistently, fecal butyrate concentrations were negatively correlated with tumor *SULF1* expression in patients with colorectal cancer (**Fig. 6F**; Supplementary Fig. S8A). There are many gut bacteria that can produce butyrate. We collected stool samples from 17 patients with colorectal cancer for third-generation 16S sequencing, among which, three reported butyrate-producing bacteria were detected (45–47). Interestingly, *Faecalibacterium prausnitzii* and *Eubacterium hallii* were negatively correlated with *SULF1* levels in tissues (**Fig. 6G**; Supplementary Fig. S8B). Cell contraction assay showed that SULF1 overexpression-induced contractility of CAFs was inhibited by butyrate supplementation (**Fig. 6H**). In addition, butyrate inhibited the hyperactivation of PI3K/AKT signaling in SULF1$^+$ CAFs (**Fig. 6I**). However, butyrate supplementation had little effect on contractility and PI3K/AKT signaling in the CAF SULF1^{KD} group (**Fig. 6J** and **K**).

Butyrate can act as an activator of G protein–coupled receptor (GPCR), or an inhibitor of HDACs (35, 48). The treatment of CAFs with pertussis toxin (a GPCR signaling inhibitor) failed to reverse the ability of butyrate to suppress *SULF1* expression, suggesting that butyrate decreases *SULF1* expression independent of its GPCR agonist activity. In contrast, the general HDAC inhibitor trichostatin A recapitulated the inhibitory effect of butyrate on *SULF1* (**Fig. 6L**), confirming that butyrate decreased *SULF1* expression in CAFs through the inhibition of HDACs. The treatment of CAFs separately with entinostat (a class I HDACi), TMP269 (a class IIa HDACi), ricolinostat (a class IIb HDACi), nicotinamide (a class III HDACi), or SIS17 (a class IV HDACi) showed that only entinostat strongly inhibited the *SULF1* expression (**Fig. 6M**). These results suggest that butyrate decreases SULF1 expression in CAFs through inhibition of class I HDACs.

SULF1$^+$ CAFs are potential indicators for patients who benefited from HDACis

To determine whether butyrate-induced SULF1 suppression in CAFs affects colorectal cancer development, the abovementioned fibroblast conditional Sulf1 knockout mice were used. Intriguingly, butyrate suppressed tumor development only in Sulf1^F WT mice but not in Sulf1^F-KO mice, suggesting that CAF-expressed Sulf1 contributed to the antitumor effect of butyrate (**Fig. 7A** and **B**). IHC experiments showed that butyrate treatment reduced the level of Sulf1 in the Sulf1-overexpressing group but not in the Sulf1-deficient group (**Fig. 7C**). Consistently, Masson staining showed that collagen components were reduced by butyrate in the Sulf1^F WT group, but not in the Sulf1^F-KO group (**Fig. 7C**). In addition, the density of CD31$^+$ blood vessels was significantly decreased by butyrate supplementation in Sulf1^F WT tumors but not in Sulf1^F-KO tumors (**Fig. 7C**; Supplementary Fig. S9A). H&E staining of the major organs revealed no obvious pathologic changes in the heart, liver, spleen, lung, kidney, or colon in any group (Supplementary Fig. S9B).

We next treated the mice with HDACi suberoylanilide hydroxamic acid (also known as vorinostat) and found that suberoylanilide hydroxamic acid reduced tumor growth (**Fig. 7D** and **E**) in mice coinjected with WT CAFs, but not those coinjected with SULF1^{KD} CAFs. The collagen deposition and the density of CD31$^+$ blood vessels showed consistent trends with tumor growth (**Fig. 7F**; Supplementary Fig. S9C). H&E staining of the major organs revealed no obvious pathologic changes in the heart, liver, spleen, lung, kidney, or colon among the different groups (Supplementary Fig. S9D). These results suggest that HDACis exert their therapeutic effect at least partially through the inhibition of SULF1 expression in CAFs.

At present, HDACis, such as chidamide, have been approved for the treatment of specific types of cancer including advanced breast cancer and peripheral T-cell lymphoma (49, 50). To further explore the clinical significance of CAF-expressed SULF1, we collected pretreatment specimens from 9 patients with breast cancer who

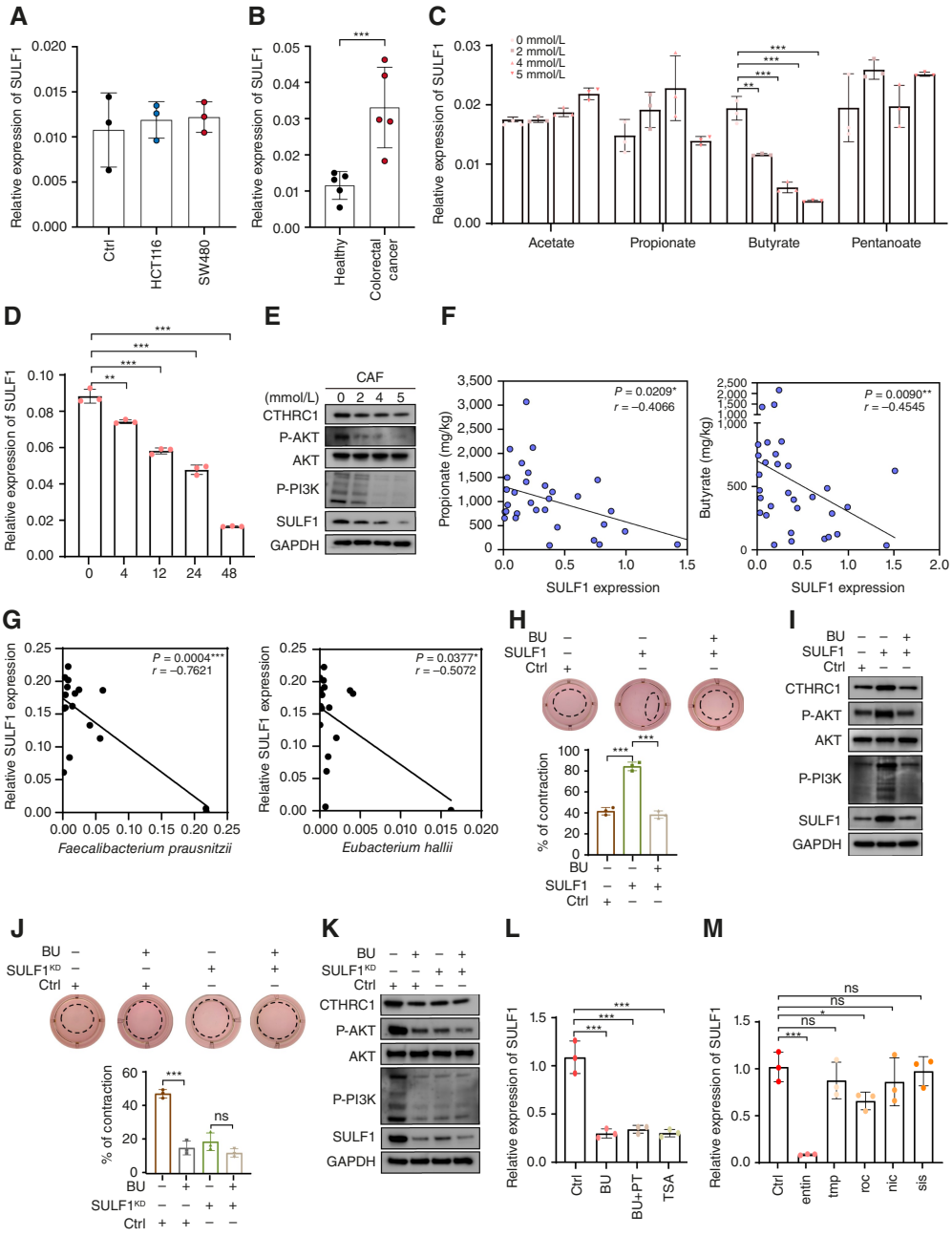

Figure 6.

SULF1 upregulation in CAFs is attributed to low butyrate production. **A,** qPCR to verify the effects of CM from HCT116 and SW480 cells on the expression of *SULF1* in CAFs. **B,** qPCR to verify the effects of fecal extracted media from healthy people and patients with colorectal cancer on the expression of *SULF1* in CAFs. **C,** qPCR to verify the effects of acetate, propionate, butyrate, and pentanoate on the expression of *SULF1* in CAFs. **D,** qPCR to detect the effects of different butyrate treatment time periods on *SULF1* levels in CAFs. **E,** Western blotting to detect the effects of butyrate at different concentrations on SULF1 levels in CAFs. **F,** Correlation between *SULF1* expression in 32 colorectal cancer tissues and the levels of SCFAs in the feces of 32 patients with colorectal cancer, as detected by qPCR. The *P* values and *r* values were determined using Spearman correlation analysis. **G,** The correlation between *SULF1* expression in 17 colorectal cancer tissues and the levels of different species of bacteria in the feces of 17 patients with colorectal cancer, as detected by qPCR. The *P* values and *r* values were determined using Spearman correlation analysis. **H,** Cell contraction assay to verify the effect of SULF1 overexpression in CAFs with/without butyrate supplementation on CAF contractility. **I,** Western blotting to verify the effect of SULF1 overexpression in CAFs with/without butyrate supplementation on PI3K/AKT signaling in CAFs. **J,** Cell contraction assay to verify the effect of knocking down/not knocking down SULF1 in CAFs with/without butyrate supplementation on the contractility of CAFs. **K,** Western blotting to verify the effect of knocking down/not knocking down SULF1 in CAFs with/without butyrate supplementation on PI3K/AKT signaling in CAFs. **L,** qPCR to detect the mRNA level of *SULF1* in CAFs in different groups. **M,** qPCR to detect the mRNA level of *SULF1* in CAFs treated with different subtypes of HDACis. The data are presented as the mean ± SD of three independent experiments, two-tailed Student *t* tests. ns, nonsignificant; **, $P < 0.01$; ***, $P < 0.001$. BU, butyrate; PT, propionate,

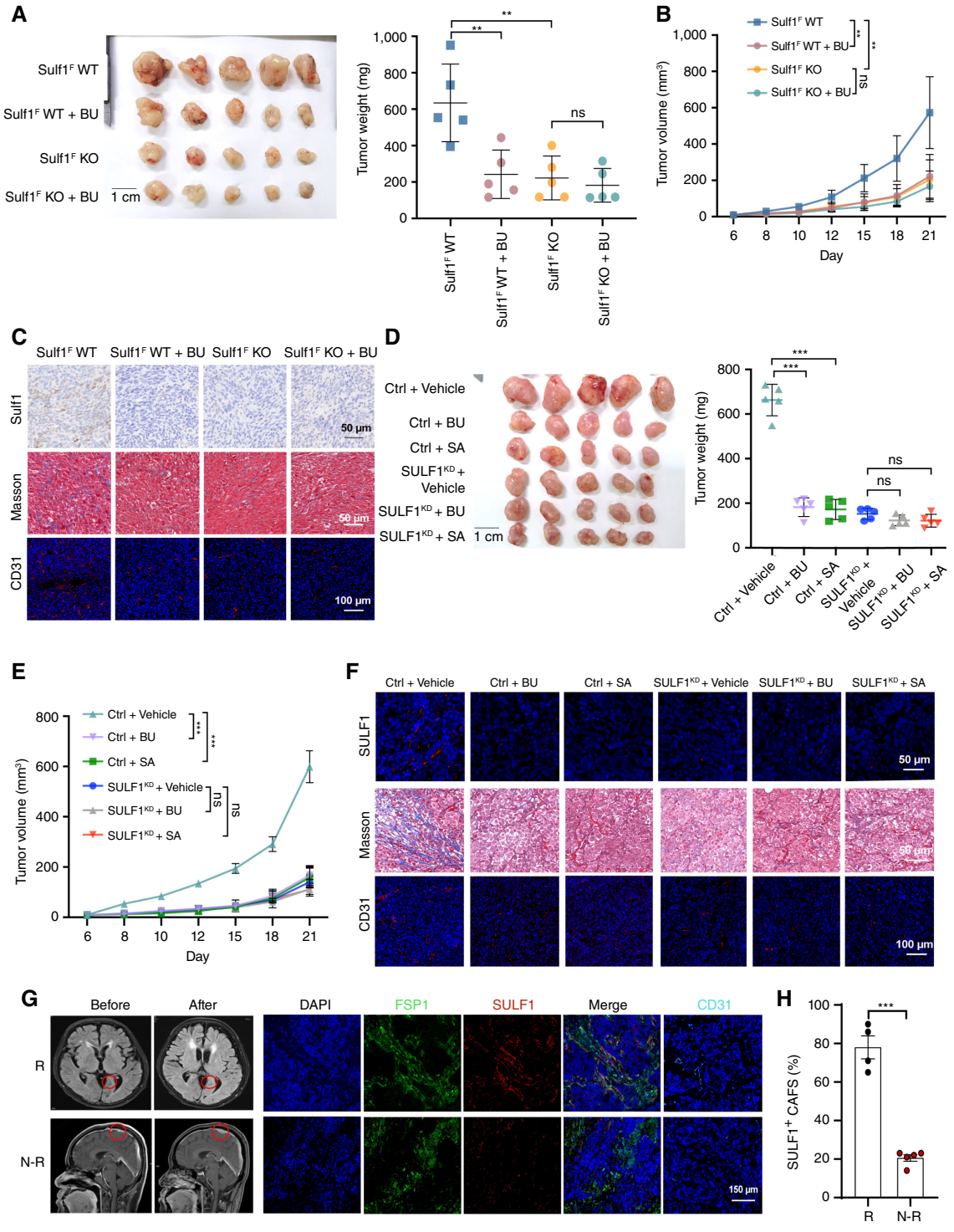

Figure 7.

SULF1 upregulation in CAFs is attributed to low butyrate production in patients with colorectal cancer. **A,** Size and weight of the subcutaneous tumorigenesis model of MC38 cells in the four groups ($n = 5$). **B,** Tumor volume in the four groups. **C,** IHC staining of Sulf1, Masson trichrome staining, and IF of CD31 in the four groups. **D,** The effect of tumor size on the subcutaneous tumorigenesis of SW480 cells in the six groups ($n = 5$). **E,** Tumor volume in the six groups. **F,** IF of SULF1, Masson trichrome staining, and IF of CD31 in the six groups. **G,** Costaining (yellow) of SULF1 and FSP1 was detected by IF staining of SULF1 (red) and FSP1 (green) in patients with advanced breast cancer (responders, $n = 4$; nonresponders $n = 5$) and by IF staining of CD31 in patients with advanced breast cancer (responders $n = 4$; nonresponders $n = 5$). **H,** Proportion of $SULF1^+$ CAFs in responders ($n = 4$) and nonresponders ($n = 5$). The data are presented as the mean ± SD of three independent experiments, two-tailed Student *t* tests. ns, nonsignificant; **, $P < 0.01$; ***, $P < 0.001$. BU, butyrate.

received chidamide therapy (chidamide in combination with exemestane). IF staining results demonstrated that SULF1 and FSP1 had substantial colocalization in breast cancer tissues, supporting the fibroblast-specific expression of SULF1. Strikingly, patients who responded to chidamide had significantly more SULF1$^+$ CAFs than the nonresponders (**Fig. 7G** and **H**); simultaneously, we also found that patients with breast cancer who had more SULF1$^+$ CAFs had relatively higher expression of CD31 (**Fig. 7G**). The results suggest that patients with more SULF1$^+$ CAFs are more likely to benefit from HDACi therapy.

Discussion

Through in-depth analysis and mining of the recently published single-cell public database of colorectal cancer (datasets GSE132465 and GSE144735; ref. 39), identified a CAF subtype with *SULF1* as the marker gene for the first time. In addition, we further verified the CAF-specific expression of SULF1 in colorectal cancer tissues through FISH and IF. FISH analyses indicated an almost perfect overlap between SULF1 and FSP expression, whereas the IF analyses suggested some SULF1- or FSP1 single-positive cells, it was expected that SULF1 and FSP1 are costained differently in FISH and IF staining because one is at the RNA level and the other is at the protein level, and our study was based on the SULF1 protein levels. Previous studies of SULF1 only focused on the effect of its expression and function in tumor cells (51, 52). In our study, we identified CAFs as the main source of SULF1 in colorectal cancer tissues. The SULF1$^+$ CAFs are closely associated with colorectal cancer progression, a finding that provides new targets for the colorectal cancer treatment.

In different research contexts, it is noteworthy that the SULF1–HSPG axis might have different effects on tumor development, depending on the type of ligands sequestered by HSPG (51, 53). In colorectal cancer, we found that SULF1$^+$ CAFs mainly impact the bioavailability of VEGFA, which activated angiogenesis in the TME. Previous studies on the regulatory effect of SULF1 on angiogenesis have shown inconsistent results. SULF1 was reported to be a critical inducer of postinfarction angiogenesis in acute myocardial infarction (54), whereas it inhibited angiogenesis and tumorigenesis *in vivo* in breast cancer (55). In our study, we demonstrated that SULF1 promoted VEGFA release from HSPG and promoted colorectal cancer angiogenesis *in vitro*, in genetically engineered mice and in human specimens.

We found that SULF1 was mainly enriched in the regulation of cell adhesion and the composition of ECM components through the VEGFA/AKT axis in CAFs. It has been reported that chemotherapy induces PIGF/VEGF upregulation, which directly activates CAFs to produce ECM in pancreatic ductal adenocarcinoma (56). In the past few years, how the ECM affects the malignant behaviors of tumor cells has emerged as the focus of tumor research (57, 58). ECM stiffness transmits mechanical signals from outside the cell to the cell through mechanical transduction pathways, such as squeezing or stretching through tension models, to cause tumor cells to have biological responses. Membrane proteins sense ECM signals, recruit downstream molecules to transmit mechanical signals, and further activate downstream pathways (59, 60). Our study provides new insights into ECM-mediated tumor regulation by revealing that SULF1 increased the secretion of the ECM protein CTHRC1, which has been reported to be related to multiple signaling pathways such as the TGFβ, WNT, and Hippo/YAP pathways (61–63). It is still possible that other pathways are involved in this process, which should be further explored.

In previous studies, SULF1 was found to be regulated by TGFβ as well as certain noncoding RNAs in tumor cells (64, 65). Our study identified a new upstream regulatory mechanism of the SULF1$^+$ subpopulation of CAFs. There is a complex relationship between tumor cells and mesenchymal cells in the TME, and tumor cells and immune cells in the stroma can promote the transformation of CAFs through various mechanisms (66, 67); however, when we used the CM from colorectal cancer tumor cells to treat CAFs, we did not observe changes in *SULF1* expression, excluding the possibility that tumor cell-derived factors modulate *SULF1* expression. Recently, the role of the gut microbiota and its metabolites in colorectal cancer has been a research hotspot and has significantly affected colorectal cancer resistance and susceptibility (68, 69). Among various microbial metabolites, SCFAs exist at high concentrations and play pivotal roles in regulating the TME by acting on tumor and immune cells (70, 71). However, the impact of SCFAs on CAFs remains elusive. Our study showed that compared with those cultured with fecal media from healthy volunteers, CAFs cultured with fecal media collected from patients with colorectal cancer had a significantly elevated *SULF1* expression. This was the first study to report the regulation of CAFs by SCFAs, which affects the function of CAFs and the expression of key genes, providing strong evidence for the contribution of SCFAs to colorectal cancer progression.

In addition, we showed for the first time that butyrate regulated the function of CAFs through HDAC inhibition and revealed that the expression level of SULF1 in CAFs determined the clinical efficacy of butyrate and HDACis, providing the possibility for CAF-targeted colorectal cancer treatment. HDACis have attracted much attention in recent decades. To date, more than 30 HDACis have been studied in clinical trials. Vorinostat was the first HDACi to receive a FDA approval for the treatment of cutaneous T-cell lymphoma in 2006 (72). Subsequently, several HDACis, such as belinostat, romidepsin, tucidinostat, and panobinostat, have been approved by the FDA for lymphoma and multiple myeloma treatment (73). Tucidinostat, also referred to as chidamide, was approved by China's National Medical Products Administration for use in peripheral T-cell lymphoma in 2014 and for use in patients with postmenopausal advanced breast cancer in combination with exemestane in 2019 (74). The role and mechanism of HDACis in solid tumors require further study. In our study, we found that there was a high proportion of SULF$^+$ CAFs in patients who responded to chidamide, suggesting that SULF1 expression may serve as a potential biomarker in HDACi-based cancer therapies. In our ongoing project, patients with colorectal cancer are involved in assessment of whether SULF1$^+$ CAFs could serve as a candidate biomarker for HDACi therapy.

This study has several limitations. For example, the specific mechanism by which ECM-related proteins regulate colorectal cancer tumor cells needs to be further explored. Furthermore, although butyrate inhibited SULF1 expression through the function of HDACis, the direct interaction mechanisms involved require further investigation. The expression of SULF1 in breast cancer and the effectiveness of chidamide treatment in our study were retrospectively studied, and the number of patients was relatively low; therefore, we can only conclude that patients with colorectal cancer and high expression of SULF1 may benefit from chidamide treatment. To further enhance the specificity of the association, we initiated a clinical study in patients with colorectal cancer to explore the specific relationship between SULF1 expression and the response to chidamide in patients with colorectal cancer. Taken together, our findings revealed the protumor capacity of SULF1$^+$ CAFs

and its potential significance in predicting the therapeutic outcome of HDACi drugs.

Authors' Disclosures

No disclosures were reported.

Authors' Contributions

H. Wang: Data curation, software, validation, investigation, methodology, writing–original draft. **J. Chen:** Methodology. **X. Chen:** Formal analysis. **Y. Liu:** Formal analysis. **J. Wang:** Formal analysis. **Q. Meng:** Formal analysis. **H. Wang:** Formal analysis. **Y. He:** Formal analysis. **Y. Song:** Investigation. **J. Li:** Formal analysis. **Z. Ju:** Writing–review and editing. **P. Xiao:** Writing–original draft, writing–review and editing. **J. Qian:** Funding acquisition, writing–original draft, writing–review and editing. **Z. Song:** Conceptualization, resources, funding acquisition, writing–original draft, project administration.

Acknowledgments

This work was partially supported by grants from the National Natural Science Foundation of China (no. 82273265 to Z. Song and no. 82303951 to J. Qian), the Zhejiang Province Research and Development Program of "Lingyan" (no. 2023C03065 to Z. Song), the Natural Science Foundation of Zhejiang Province (LQ24160004 to J. Chen), and the Zhejiang Province Natural Science Fund for Excellent Young Scholars (LR22H160004 to J. Qian).

Note

Supplementary data for this article are available at Cancer Research Online (http://cancerres.aacrjournals.org/).

Received December 15, 2023; revised April 18, 2024; accepted July 16, 2024; published first September 9, 2024.

References

1. Kratzer TB, Jemal A, Miller KD, Nash S, Wiggins C, Redwood D, et al. Cancer statistics for American Indian and Alaska Native Individuals, 2022: including increasing disparities in early onset colorectal cancer. CA Cancer J Clin 2023;73:120–46.
2. Siegel RL, Miller KD, Fuchs HE, Jemal A. Cancer statistics, 2022. CA Cancer J Clin 2022;72:7–33.
3. El Zarif T, Yibirin M, De Oliveira-Gomes D, Machaalani M, Nawfal R, Bittar G, et al. Overcoming therapy resistance in colon cancer by drug repurposing. Cancers (Basel) 2022;14:2105.
4. Miller KD, Nogueira L, Devasia T, Mariotto AB, Yabroff KR, Jemal A, et al. Cancer treatment and survivorship statistics, 2022. CA Cancer J Clin 2022;72:409–36.
5. Benson AB, Venook AP, Al-Hawary MM, Arain MA, Chen YJ, Ciombor KK, et al. Colon cancer, version 2.2021, NCCN Clinical Practice Guidelines in Oncology. J Natl Compr Canc Netw 2021;19:329–59.
6. Rimal R, Desai P, Daware R, Hosseinnejad A, Prakash J, Lammers T, et al. Cancer-associated fibroblasts: origin, function, imaging, and therapeutic targeting. Adv Drug Deliv Rev 2022;189:114504.
7. Houthuijzen JM, de Bruijn R, van der Burg E, Drenth AP, Wientjens E, Filipovic T, et al. CD26-negative and CD26-positive tissue-resident fibroblasts contribute to functionally distinct CAF subpopulations in breast cancer. Nat Commun 2023;14:183.
8. Peng S, Li Y, Huang M, Tang G, Xie Y, Chen D, et al. Metabolomics reveals that CAF-derived lipids promote colorectal cancer peritoneal metastasis by enhancing membrane fluidity. Int J Biol Sci 2022;18:1912–32.
9. Papanicolaou M, Parker AL, Yam M, Filipe EC, Wu SZ, Chitty JL, et al. Temporal profiling of the breast tumour microenvironment reveals collagen XII as a driver of metastasis. Nat Commun 2022;13:4587.
10. Zhuang J, Shen L, Li M, Sun J, Hao J, Li J, et al. Cancer-associated fibroblast-derived miR-146a-5p generates a niche that promotes bladder cancer stemness and chemoresistance. Cancer Res 2023;83:1611–27.
11. Affo S, Nair A, Brundu F, Ravichandra A, Bhattacharjee S, Matsuda M, et al. Promotion of cholangiocarcinoma growth by diverse cancer-associated fibroblast subpopulations. Cancer Cell 2021;39:883.
12. Rapetti-Mauss R, Nigri J, Berenguier C, Finetti P, Tubiana SS, Labrum B, et al. SK2 channels set a signalling hub bolstering CAF-triggered tumourigenic processes in pancreatic cancer. Gut 2023;72:722–35.
13. Mizutani Y, Kobayashi H, Iida T, Asai N, Masamune A, Hara A, et al. Meflin-positive cancer-associated fibroblasts inhibit pancreatic carcinogenesis. Cancer Res 2019;79:5367–81.
14. Kochetkova M, Samuel MS. Differentiation of the tumor microenvironment: are CAFs the organizer? Trends Cell Biol 2022;32:285–94.
15. Chen Z, Zhou L, Liu L, Hou Y, Xiong M, Yang Y, et al. Single-cell RNA sequencing highlights the role of inflammatory cancer-associated fibroblasts in bladder urothelial carcinoma. Nat Commun 2020;11:5077.
16. Hutton C, Heider F, Blanco-Gomez A, Banyard A, Kononov A, Zhang X, et al. Single-cell analysis defines a pancreatic fibroblast lineage that supports anti-tumor immunity. Cancer Cell 2021;39:1227–44.e20.
17. Yu L, Shen N, Shi Y, Shi X, Fu X, Li S, et al. Characterization of cancer-related fibroblasts (CAF) in hepatocellular carcinoma and construction of CAF-based risk signature based on single-cell RNA-seq and bulk RNA-seq data. Front Immunol 2022;13:1009789.
18. André C, Lethier L, Adotevi O, Guillaume YC. Development of a new heparan sulfate proteoglycan (HSPG) chromolith LC column to study the pH dependence binding of peptide vaccines to HSPG and role of human serum albumin on its binding. Anal Methods 2023;15:1323–35.
19. Araujo AP, Ribeiro ME, Ricci R, Torquato RJ, Toma L, Porcionatto MA. Glial cells modulate heparan sulfate proteoglycan (HSPG) expression by neuronal precursors during early postnatal cerebellar development. Int J Dev Neurosci 2010;28:611–20.
20. Eguchi Y, Inoue M, Iida S, Matsuoka K, Noda S. Heparan sulfate (HS)/heparan sulfate proteoglycan (HSPG) and bikunin are up-regulated during calcium oxalate nephrolithiasis in rat kidney. Kurume Med J 2002;49:99–107.
21. Ergezen E, Hong S, Barbee KA, Lec R. Real time monitoring of the effects of heparan sulfate proteoglycan (HSPG) and surface charge on the cell adhesion process using thickness shear mode (TSM) sensor. Biosens Bioelectron 2007;22:2256–60.
22. He X, Khurana A, Roy D, Kaufmann S, Shridhar V. Loss of HSulf-1 expression enhances tumorigenicity by inhibiting Bim expression in ovarian cancer. Int J Cancer 2014;135:1783–9.
23. Lai JP, Chien J, Strome SE, Staub J, Montoya DP, Greene EL, et al. HSulf-1 modulates HGF-mediated tumor cell invasion and signaling in head and neck squamous carcinoma. Oncogene 2004;23:1439–47.
24. Lai JP, Yu C, Moser CD, Aderca I, Han T, Garvey TD, et al. SULF1 inhibits tumor growth and potentiates the effects of histone deacetylase inhibitors in hepatocellular carcinoma. Gastroenterology 2006;130:2130–44.
25. Zhao H, Chen Z, Fang Y, Su M, Xu Y, Wang Z, et al. Prediction of prognosis and recurrence of bladder cancer by ECM-related genes. J Immunol Res 2022;2022:1793005.
26. Lee HY, Yeh BW, Chan TC, Yang KF, Li WM, Huang CN, et al. Sulfatase-1 overexpression indicates poor prognosis in urothelial carcinoma of the urinary bladder and upper tract. Oncotarget 2017;8:47216–29.
27. Ganapathy V, Thangaraju M, Prasad PD, Martin PM, Singh N. Transporters and receptors for short-chain fatty acids as the molecular link between colonic bacteria and the host. Curr Opin Pharmacol 2013;13:869–74.
28. Miller TL, Wolin MJ. Pathways of acetate, propionate, and butyrate formation by the human fecal microbial flora. Appl Environ Microbiol 1996;62:1589–92.
29. Bartolomaeus H, Balogh A, Yakoub M, Homann S, Markó L, Höges S, et al. Short-chain fatty acid propionate protects from hypertensive cardiovascular damage. Circulation 2019;139:1407–21.
30. Deleu S, Machiels K, Raes J, Verbeke K, Vermeire S. Short chain fatty acids and its producing organisms: an overlooked therapy for IBD? EBioMedicine 2021;66:103293.
31. Guo W, Zhang Z, Li L, Liang X, Wu Y, Wang X, et al. Gut microbiota induces DNA methylation via SCFAs predisposing obesity-prone individuals to diabetes. Pharmacol Res 2022;182:106355.
32. Wu Z, Huang S, Li T, Li N, Han D, Zhang B, et al. Gut microbiota from green tea polyphenol-dosed mice improves intestinal epithelial homeostasis and ameliorates experimental colitis. Microbiome 2021;9:184.
33. Le Poul E, Loison C, Struyf S, Springael JY, Lannoy V, Decobecq ME, et al. Functional characterization of human receptors for short chain fatty acids and

their role in polymorphonuclear cell activation. J Biol Chem 2003;278:25481–9.
34. Singh N, Gurav A, Sivaprakasam S, Brady E, Padia R, Shi H, et al. Activation of Gpr109a, receptor for niacin and the commensal metabolite butyrate, suppresses colonic inflammation and carcinogenesis. Immunity 2014;40:128–39.
35. Thangaraju M, Cresci GA, Liu K, Ananth S, Gnanaprakasam JP, Browning DD, et al. GPR109A is a G-protein-coupled receptor for the bacterial fermentation product butyrate and functions as a tumor suppressor in colon. Cancer Res 2009;69:2826–32.
36. Qian J, Olbrecht S, Boeckx B, Vos H, Laoui D, Etlioglu E, et al. A pan-cancer blueprint of the heterogeneous tumor microenvironment revealed by single-cell profiling. Cell Res 2020;30:745–62.
37. He Y, Ling Y, Zhang Z, Mertens RT, Cao Q, Xu X, et al. Butyrate reverses ferroptosis resistance in colorectal cancer by inducing c-Fos-dependent xCT suppression. Redox Biol 2023;65:102822.
38. Fumagalli A, Suijkerbuijk SJE, Begthel H, Beerling E, Oost KC, Snippert HJ, et al. A surgical orthotopic organoid transplantation approach in mice to visualize and study colorectal cancer progression. Nat Protoc 2018;13:235–47.
39. Lee HO, Hong Y, Etlioglu HE, Cho YB, Pomella V, Van den Bosch B, et al. Lineage-dependent gene expression programs influence the immune landscape of colorectal cancer. Nat Genet 2020;52:594–603.
40. Lambert AW, Weinberg RA. Linking EMT programmes to normal and neoplastic epithelial stem cells. Nat Rev Cancer 2021;21:325–38.
41. Zhang N, Ng AS, Cai S, Li Q, Yang L, Kerr D. Novel therapeutic strategies: targeting epithelial-mesenchymal transition in colorectal cancer. Lancet Oncol 2021;22:e358–68.
42. Bishop JR, Schuksz M, Esko JD. Heparan sulphate proteoglycans fine-tune mammalian physiology. Nature 2007;446:1030–7.
43. Hayashida K, Aquino RS, Park PW. Coreceptor functions of cell surface heparan sulfate proteoglycans. Am J Physiol Cell Physiol 2022;322:C896–912.
44. Danne C, Sokol H. Butyrate, a new microbiota-dependent player in CD8$^+$ T cells immunity and cancer therapy? Cell Rep Med 2021;2:100328.
45. Machiels K, Joossens M, Sabino J, De Preter V, Arijs I, Eeckhaut V, et al. A decrease of the butyrate-producing species Roseburia hominis and Faecalibacterium prausnitzii defines dysbiosis in patients with ulcerative colitis. Gut 2014;63:1275–83.
46. Moens F, Verce M, De Vuyst L. Lactate- and acetate-based cross-feeding interactions between selected strains of lactobacilli, bifidobacteria and colon bacteria in the presence of inulin-type fructans. Int J Food Microbiol 2017;241:225–36.
47. Lu H, Xu X, Fu D, Gu Y, Fan R, Yi H, et al. Butyrate-producing Eubacterium rectale suppresses lymphomagenesis by alleviating the TNF-induced TLR4/MyD88/NF-κB axis. Cell Host Microbe 2022;30:1139–50.e7.
48. Waldecker M, Kautenburger T, Daumann H, Busch C, Schrenk D. Inhibition of histone-deacetylase activity by short-chain fatty acids and some polyphenol metabolites formed in the colon. J Nutr Biochem 2008;19:587–93.
49. Shi Y, Jia B, Xu W, Li W, Liu T, Liu P, et al. Chidamide in relapsed or refractory peripheral T cell lymphoma: a multicenter real-world study in China. J Hematol Oncol 2017;10:69.
50. Tu K, Yu Y, Wang Y, Yang T, Hu Q, Qin X, et al. Combination of chidamide-mediated epigenetic modulation with immunotherapy: boosting tumor immunogenicity and response to PD-1/PD-L1 blockade. ACS Appl Mater Interfaces 2021;13:39003–17.
51. Li J, Mo ML, Chen Z, Yang J, Li QS, Wang DJ, et al. HSulf-1 inhibits cell proliferation and invasion in human gastric cancer. Cancer Sci 2011;102:1815–21.
52. Vicente CM, Lima MA, Yates EA, Nader HB, Toma L. Enhanced tumorigenic potential of colorectal cancer cells by extracellular sulfatases. Mol Cancer Res 2015;13:510–23.
53. Dhanasekaran R, Nakamura I, Hu C, Chen G, Oseini AM, Seven ES, et al. Activation of the transforming growth factor-β/SMAD transcriptional pathway underlies a novel tumor-promoting role of sulfatase 1 in hepatocellular carcinoma. Hepatology 2015;61:1269–83.
54. Korf-Klingebiel M, Reboll MR, Grote K, Schleiner H, Wang Y, Wu X, et al. Heparan sulfate-editing extracellular sulfatases enhance VEGF bioavailability for ischemic heart repair. Circ Res 2019;125:787–801.
55. Narita K, Staub J, Chien J, Meyer K, Bauer M, Friedl A, et al. HSulf-1 inhibits angiogenesis and tumorigenesis in vivo. Cancer Res 2006;66:6025–32.
56. Kim DK, Jeong J, Lee DS, Hyeon DY, Park GW, Jeon S, et al. PD-L1-directed PlGF/VEGF blockade synergizes with chemotherapy by targeting CD141$^+$ cancer-associated fibroblasts in pancreatic cancer. Nat Commun 2022;13:6292.
57. Huang J, Zhang L, Wan D, Zhou L, Zheng S, Lin S, et al. Extracellular matrix and its therapeutic potential for cancer treatment. Signal Transduct Target Ther 2021;6:153.
58. Wu B, Liu DA, Guan L, Myint PK, Chin L, Dang H, et al. Stiff matrix induces exosome secretion to promote tumour growth. Nat Cell Biol 2023;25:415–24.
59. Jiang Y, Zhang H, Wang J, Liu Y, Luo T, Hua H. Targeting extracellular matrix stiffness and mechanotransducers to improve cancer therapy. J Hematol Oncol 2022;15:34.
60. Mohan V, Das A, Sagi I. Emerging roles of ECM remodeling processes in cancer. Semin Cancer Biol 2020;62:192–200.
61. Chen YL, Wang TH, Hsu HC, Yuan RH, Jeng YM. Overexpression of CTHRC1 in hepatocellular carcinoma promotes tumor invasion and predicts poor prognosis. PLoS One 2013;8:e70324.
62. Huang D, Du X. Crosstalk between tumor cells and microenvironment via Wnt pathway in colorectal cancer dissemination. World J Gastroenterol 2008;14:1823–7.
63. Pyagay P, Heroult M, Wang Q, Lehnert W, Belden J, Liaw L, et al. Collagen triple helix repeat containing 1, a novel secreted protein in injured and diseased arteries, inhibits collagen expression and promotes cell migration. Circ Res 2005;96:261–8.
64. Bao L, Yan Y, Xu C, Ji W, Shen S, Xu G, et al. MicroRNA-21 suppresses PTEN and hSulf-1 expression and promotes hepatocellular carcinoma progression through AKT/ERK pathways. Cancer Lett 2013;337:226–36.
65. Pham TP, van Bergen AS, Kremer V, Glaser SF, Dimmeler S, Boon RA. LncRNA AERRIE is required for sulfatase 1 expression, but not for endothelial-to-mesenchymal transition. Int J Mol Sci 2021;22:8088.
66. Mao X, Xu J, Wang W, Liang C, Hua J, Liu J, et al. Crosstalk between cancer-associated fibroblasts and immune cells in the tumor microenvironment: new findings and future perspectives. Mol Cancer 2021;20:131.
67. Sahai E, Astsaturov I, Cukierman E, DeNardo DG, Egeblad M, Evans RM, et al. A framework for advancing our understanding of cancer-associated fibroblasts. Nat Rev Cancer 2020;20:174–86.
68. Garrett WS. The gut microbiota and colon cancer. Science 2019;364:1133–5.
69. Song M, Chan AT, Sun J. Influence of the gut microbiome, diet, and environment on risk of colorectal cancer. Gastroenterology 2020;158:322–40.
70. Guo C, Guo D, Fang L, Sang T, Wu J, Guo C, et al. Ganoderma lucidum polysaccharide modulates gut microbiota and immune cell function to inhibit inflammation and tumorigenesis in colon. Carbohydr Polym 2021;267:118231.
71. Malik A, Sharma D, Malireddi RKS, Guy CS, Chang TC, Olsen SR, et al. SYK-CARD9 signaling axis promotes gut fungi-mediated inflammasome activation to restrict colitis and colon cancer. Immunity 2018;49:515–30.e5.
72. Marks PA, Breslow R. Dimethyl sulfoxide to vorinostat: development of this histone deacetylase inhibitor as an anticancer drug. Nat Biotechnol 2007;25:84–90.
73. Ho TCS, Chan AHY, Ganesan A. Thirty years of HDAC inhibitors: 2020 insight and hindsight. J Med Chem 2020;63:12460–84.
74. Jiang Z, Li W, Hu X, Zhang Q, Sun T, Cui S, et al. Tucidinostat plus exemestane for postmenopausal patients with advanced, hormone receptor-positive breast cancer (ACE): a randomised, double-blind, placebo-controlled, phase 3 trial. Lancet Oncol 2019;20:806–15.